A GENERALIZED FINITE ELEMENT METHOD FOR EARTH RETURN IMPEDANCE AND ADMITTANCE IN VERTICALLY-MULTILAYERED MEDIA

LUCAS SANTOS LESSA

DISSERTAÇÃO DE MESTRADO
EM ENGENHARIA ELÉTRICA

DEPARTAMENTO DE ENGENHARIA ELÉTRICA

FACULDADE DE TECNOLOGIA

UNIVERSIDADE DE BRASÍLIA

Universidade de Brasília
Faculdade de Tecnologia
Departamento de Engenharia Elétrica

A Generalized Finite Element Method for Earth Return Impedance and Admittance in Vertically-Multilayered Media

Lucas Santos Lessa

DISSERTAÇÃO DE MESTRADO SUBMETIDA AO PROGRAMA DE PÓS-GRADUAÇÃO EM ENGENHARIA ELÉTRICA DA UNIVERSIDADE DE BRASÍLIA COMO PARTE DOS REQUISITOS NECESSÁRIOS PARA A OBTENÇÃO DO GRAU DE MESTRE.

APROVADA POR:

Prof. Kleber Melo e Silva, D.Sc. (ENE-UnB)
(Orientador)

Prof. Felipe Vigolvino Lopes, D.Sc. (UFCG)
(Examinador Externo)

Prof. Alberto Resende De Conti, D.Sc. (UFMG)
(Examinador Externo)

Brasília/DF, Dezembro de 2025.

FICHA CATALOGRÁFICA

SANTOS, LUCAS

A Generalized Finite Element Method for Earth Return Impedance and Admittance in Vertically-Multilayered Media. [Brasília/DF] 2025.

xxx, nnnp., 210 x 297 mm (ENE/FT/UnB, Mestre, Dissertação de Mestrado, 2025).

Universidade de Brasília, Faculdade de Tecnologia, Departamento de Engenharia Elétrica.

Departamento de Engenharia Elétrica

1. Vertically Stratified Soil
2. Finite Element Method (FEM)
3. Earth-Return Impedance
4. Earth-Return Admitance
5. Frequency-Dependent Parameters
6. Electromagnetic Transients
7. HVDC Submarine
8. Electromagnetic Interference (EMI)

I. ENE/FT/UnB

II. Título (série)

REFERÊNCIA BIBLIOGRÁFICA

SANTOS, LUCAS (2025). A Generalized Finite Element Method for Earth Return Impedance and Admittance in Vertically-Multilayered Media. Dissertação de Mestrado, Publicação PPGEE.837/2025, Departamento de Engenharia Elétrica, Universidade de Brasília, Brasília, DF, 76.

CESSÃO DE DIREITOS

AUTOR: Lucas Santos

TÍTULO: A Generalized Finite Element Method for Earth Return Impedance and Admittance in Vertically-Multilayered Media.

GRAU: Mestre ANO: 2025

Lucas Santos

Universidade de Brasília (UnB)

Campus Darcy Ribeiro

Faculdade de Tecnologia - FT

Departamento de Engenharia Elétrica(ENE)

Brasília - DF CEP 70919-970

To the reader.

AGRADECIMENTOS

Primeiramente eu gostaria de agradecer ao Prof. Amauri pela orientação durante esse trabalho.

Agradeço ao Prof. Kleber pelo apoio contínuo e paciência durante o desenvolvimento desta pesquisa. Suas valiosas contribuições na revisão do texto, sempre feitas com disposição e respeito, foram fundamentais para a conclusão deste trabalho.

A minha família pelo apoio e incentivo constante.

À Universidade de Brasília - UnB por tudo que ela me proporcionou.

E enfim, mas, não menos importante, a Deus.

RESUMO

Título: Um Método de Elementos Finitos Generalizado para Impedância de Retorno à Terra e Admitância em Meios Multicamadas Verticais

Este trabalho descreve o problema da modelagem precisa de parâmetros de cabos aéreos e subterrâneos (impedâncias e admitâncias de retorno pela terra) para estudos de interferência eletromagnética (IEM) em solos lateralmente estratificados. É desenvolvida uma ferramenta computacional avançada baseada no Método dos Elementos Finitos (MEF), utilizando uma cadeia de ferramentas de código aberto (`LineCableLab`, `LineCableModels.jl`, `GetDP`, `Gmsh`).

A metodologia proposta supera as limitações dos modelos magnetostáticos tradicionais ao empregar uma formulação eletrodinâmica completa, que inclui a permissividade do material e uma transformação de domínio de casca infinita. Isso permite o cálculo de parâmetros fisicamente consistentes em um amplo espectro de frequências (0,1 Hz a 1 MHz). Os códigos são validados por meio de estudos de caso e comparações com dados de fabricantes de cabos. A ferramenta é aplicada a cenários complexos, como um cabo submarino HVDC de 525 kV, e em simulações de transientes no PSCAD, demonstrando a importância da modelagem detalhada para a correta avaliação de riscos.

Este trabalho é de interesse prático para as indústrias de energia elétrica, óleo e gás, e de energias renováveis (eólica offshore), contribuindo com o desenvolvimento de técnicas avançadas para prever e mitigar riscos em projetos que envolvam acoplamento eletromagnético em solos complexos.

Palavras-chave: Método dos Elementos Finitos (MEF), Impedância de Retorno à Terra, Admitância de Retorno à Terra, Solo Estratificado Verticalmente, Parâmetros Dependentes da Frequência, Cabos Submarinos HVDC, Interferência Eletromagnética (EMI), Transitórios Eletromagnéticos

ABSTRACT

This work describes the problem of accurately modeling overhead and underground cable parameters (ground return impedances and admittances) for electromagnetic interference (EMI) studies in laterally stratified soils. An advanced computational tool based on the Finite Element Method (FEM) is developed, using a chain of open source tools (`LineCableLab`, `LineCableModels.jl`, `GetDP`, `Gmsh`).

The proposed methodology overcomes the limitations of traditional magnetostatic models by employing a complete electrodynamic formulation, which includes material permittivity and an infinite shell domain transformation. This allows the calculation of physically consistent parameters over a wide frequency spectrum (0.1 Hz to 1 MHz). The codes are validated through case studies and comparisons with data from cable manufacturers. The tool is applied to complex scenarios, such as a 525 kV HVDC submarine cable, and in transient simulations in PSCAD, demonstrating the importance of detailed modeling for correct risk assessment.

This work is of practical interest to the electric power, oil and gas, and renewable energy (offshore wind) industries, contributing to the development of advanced techniques for predicting and mitigating risks in projects involving electromagnetic coupling in complex soils.

Keywords: Finite Element Method (FEM), Earth-Return Impedance, Earth-Return Admittance, Vertically Stratified Soil, Frequency-Dependent Parameters, HVDC Submarine Cables, Electromagnetic Interference (EMI), Electromagnetic Transients

CONTENTS

LIST OF FIGURES

LIST OF TABLES

LIST OF SYMBOLS

ε_r	Relative electric permittivity	[p.u.]
ρ	Electrical resistivity [Ω·m]	
R_a	Apparent resistance [Ω]	
I_{AB}	Test current between terminals A and B in the Wenner array [A]	
V_{CD}	Voltage drop between terminals C and D in the Wenner array [V]	
a	Electrode spacing in the Wenner array [m]	
b	Electrode insertion depth in the Wenner array [m]	
ϵ	Electric permittivity [F/m]	
μ	Magnetic permeability [H/m]	
I	Electric current [A]	
$Z_{i,j}$	Mutual impedance between conductors i and j [Ω/m]	
ω	System angular frequency [rad/s]	
ϵ_0	Vacuum electric permittivity ($\approx 8.85 \times 10^{-12}$) [F/m]	
μ_0	Free space magnetic permeability ($= 4\pi \times 10^{-7}$) [H/m]	
$Z_{i,i}$	Self impedance of conductor i [Ω/m]	
r_{ext}	Conductor external radius [m]	
r_{ef}	Effective radius of conductor or bundle [m]	
$P_{i,i}$	Self potential coefficient of conductor i [m/F]	
Z	Series impedance [Ω]	

Y	Shunt admittance [S]
$\boldsymbol{J}_i$	Impressed current density vector [A/m^2]

GLOSSARY

3LPE	Three-layer polyethylene
AC	Alternating current
ATP	Alternative Transient Program
EMI	Electromagnetic interference
ETL	Extended Transmission Line
FEM	Finite element method
FEMM	Finite Element Method Magnetics
GetDP	General environment for the Treatment of Discrete Problems
GPR	Ground potential rise
HVDC	High Voltage Direct Current
IEEE	Institute of Electrical and Electronics Engineers
LCC	Line Cable Constants
MATLAB	Matrix Laboratory
MQS	Magnetoquasistatic
NACE	National Association of Corrosion Engineers
OHL	Overhead Line
PSCAD	Power System Computer-Aided Design
RMS	Root Mean Square
RMSD	Root Mean Square Deviation
ULM	Universal Line Model

CHAPTER 1

INTRODUCTION

1.1 PREFACE

Electromagnetic interference (EMI) encompasses interactions between transmission lines and nearby structures like pipelines, substations, and railways. Assessing EMI is crucial for determining safety levels, as induced voltages and currents can create hazardous touch, step voltages and insulation stresses, potentially compromising equipment integrity and worker safety. EMI studies consider key engineering variables to ensure design compliance with safety standards. Realistic simulation models enable cost-effective, optimized solutions that manage uncertainties and balance cost control with safety by minimizing unnecessary mitigation.

Over the years, EMI studies have advanced through innovations and more realistic approaches (HAUBRICH *et al.*, 1994; WG-36.02, 1995; DOMMEL; ADMINISTRATION, 1986). Self- and mutual-earth return impedances, along with earth-return admittances, are central to EMI, directly influencing induced voltages and currents. Established practices for EMI between overhead lines (OHL) and pipelines largely rely on foundational work by Carson and Pollaczek (1926) (CARSON, 1926; POLLACZEK, 1926), where Carson derived coupling effects for overhead conductors and Pollaczek developed impedance and admittance formulas for underground conductors.

However, Carson and Pollaczek's formulas impose constraints, omitting certain electromagnetic properties of air and earth for simplification purpose, particularly displacement currents related to earth permittivity (AMETANI *et al.*, 2022). Subsequent refinements by Wise, Wait, Kikuchi, Papadopoulos, Xue, and others (Wise, 1934; WAIT, 1972; Kikuchi, 1956; Papadopoulos *et al.*, 2010; XUE *et al.*, 2018a) have addressed these limitations. The recent Martins-Papadopoulos-Chrysochos formulations (MARTINS-BRITTO *et al.*, 2024) account for air and soil electromagnetic properties with minimal assumptions, allowing precise mutual coupling

computations between overhead lines and underground pipes, but like all the analytical formulations consider zero for the propagation constant.

While these earth formulations are valid for various applications, they generally assume homogeneous earth, which does not fully reflect real-world conditions, as natural soils often exhibit horizontal layering—known to introduce uncertainties in line parameter studies (MARTINS-BRITTO CAIO M; RONDINEAU, 2020). Significant research has focused on modeling horizontally-layered soils (NAKAGAWA *et al.*, 1973; WEDEPOHL; WASLEY, 1966; DERI *et al.*, 1981). However, lateral (i.e., vertically-layered) variations in earth resistivity remain scarcely reported due to formulation complexity, a gap that becomes particularly evident when considering the data from in-field soil measurements.

Standard procedures, such as the Wenner method (WENNER, 1916), are widely used in field surveys to measure soil resistivity. This method relies on acquiring apparent resistance values, which are then processed to estimate the resistivity representative of a localized region. Multiple measurements are typically conducted to ensure accuracy across the transmission line site. In pipeline engineering, soil resistivity measurements are essential for assessing corrosion risks and designing cathodic protection systems (Martins-Britto, 2017). In shared corridors, electromagnetic interference can be significant, particularly in regions where the installations cross or are within a few hundred meters of one another (WG-36.02, 1995). Given the heterogeneous of natural soils, substantial deviations in resistivity values are expected between transmission line and pipeline sites, which this can be best modeled using vertical soil layers, which is the focus of this work. To realistically assess electromagnetic coupling effects in such cases, a vertically stratified soil model offers a more detailed representation of local interactions between the facilities. This theoretical gap about vertical layers is significant, as standard field measurements routinely encounter these exact lateral variations in shared corridors, highlighting the practical need for a more robust numerical method capable of handling this geometric complexity.

Therefore, to address this practical need, a robust numerical method capable of handling such complex geometries is required. In this work will be used Finite Element Methods (FEM) to address the vertically stratified soil due to the generic approach. The FEM is an effective numerical tool for solving electromagnetic field equations in complex geometries (MEEKER,

2020). In a FEM-based, the line parameters of interest can be extracted from the magnetic vector potential (A) and current density integrals within conductors (PAPAGIANNIS *et al.*, 2000; PAPAGIANNIS *et al.*, 2005).

1.2 OBJECTIVES AND SCOPE

The main objective of this research is to develop a FEM calculation to model lateral stratification of the soil resistivity within shared right-of-way corridors occupied by transmission lines and pipelines.

This main objective can be divided into the following specific objectives:

1. Development and verification of a computational model capable of representing lateral soil stratification using canonical test cases and realistic engineering scenarios using FEM.
2. Development of an Enhanced FEM formulation that models the physical phenomenon of a transmission line for lateral soil stratification using `GetDP`.
3. Analysis and quantification of the impact of lateral soil heterogeneity on induced voltages and currents in coupled pipelines.
4. Transient investigation of the effect of lateral soil stratification in an HVDC system.

1.3 CONTRIBUTIONS AND DISSEMINATION

First, this thesis extends the computational capabilities in the soil model of the `LineCableLab` toolbox (MARTINS-BRITTO *et al.*, 2023) to analyze electromagnetic phenomena in vertically stratified soil environments. By integrating the finite element solver FEMM (MEEKER, 2020), the developed module overcomes the geometric limitations of traditional horizontally layered models. This enhancement allows for the rigorous determination of earth return impedance and admittance in scenarios where lateral soil heterogeneity significantly impacts the electromagnetic field distribution. This contributions culminate in a generalized FEM-based methodology for calculating earth return parameters in complex, heterogeneous soil structures. This research

was recognized with the Best Paper Award in Power Systems at the 2024 Workshop on Communication Networks and Power Systems (WCNPS) and resulted in the following peer-reviewed publication:

1. L. S. Lessa, M. A. B. Ribeiro and A. G. Martins-Britto, "A generalized FEM-based framework for earth return impedance calculations on vertically-multilayered media," 2024 Workshop on Communication Networks and Power Systems (WCNPS), Brasilia, Brazil, 2024, pp. 1-7, doi: 10.1109/WCNPS65035.2024.10814187.

Second, a high-performance numerical interface was developed to couple the General environment for the treatment of discrete problems (`GetDP`) with the `LineCableModels` toolbox (MARTINS, 2025) via the Julia language. This integration implements a magnetoquasistatic $\vec{A} - V$ formulation for the extraction of series impedance, alongside an electrodynamic formulation for shunt admittance. Collectively designated as the Enhanced Formulation, this approach rectifies the theoretical approximations inherent in preceding formulations, ensuring a more physically complete representation of the line parameters.

1.4 THESIS STRUCTURE

This work is composed of three main chapters.

Chapter 2 presents literature review of the existing formulations. It begins by reviewing the basic fundamentals of electromagnetic interference (EMI) and then presents a the existing formulations for calculating transmission line parameters in vertically layered soil models.

Chapter 3 establishes the theoretical foundations of the baseline FEMM formulation. Additionally, it details the analytical benchmark employed to validate the numerical results, ensuring the accuracy of the proposed methods.

Chapter 4 introduces the *Enhanced Formulation*, which extends the capabilities of the standard FEM approach. This chapter addresses the limitations of the baseline model, incorporating more complex physical phenomena to ensure rigorous applicability in broad frequency ranges.

Chapter 5 presents the numerical results across three distinct scenarios: a fundamental

case, a practical application case, and a HVDC system case. In all instances, the analysis focuses on quantifying the impact of lateral soil stratification on the earth return parameters.

Chapter 6 synthesizes the conclusions drawn from this research and outlines potential avenues for future work.

CHAPTER 2

LITERATURE REVIEW

Transmission Line parameters are fundamental for a wide range of power system studies, including load flow, system stability, power quality, and the analysis of electromagnetic interference (EMI) in nearby metallic structures. These parameters are primarily divided into the series impedance (Z) and the shunt admittance (Y). The modeling of both parameters is critically dependent on the path that the series and shunt currents take as they return through the earth. Consequently, the electrical properties of the soil play a crucial role in the accurate calculation of these earth return parameters. Figure 2.1 illustrates the equivalent circuit representation of a transmission line section.

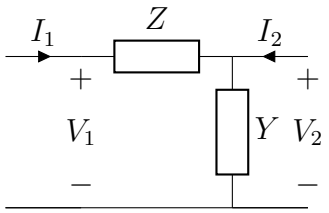

Figure 2.1. Equivalent circuit model representing the series impedance and shunt admittance.

2.1 SOIL MODEL

Natural soil structures exhibit inherent heterogeneity, characterized by the spatial variation of electromagnetic properties such as resistivity and permittivity (TODD, 2006). In contrast to this physical reality, classical analytical formulations, most notably the works of Carson and Pollaczek, rely on the simplifying assumption of a homogeneous half-space, while often neglecting displacement currents (permittivity). Consequently, these early models limit the accuracy of high-frequency or complex-terrain analysis. To overcome these drawbacks modeling techniques have evolved to represent the soil in a more realistic manner, accounting for both vertical stratification and frequency-dependent parameters.

Scott *et al.* (1964) investigated the dependence of soil permittivity on key environmental variables, including moisture content, frequency, and soil composition. The authors addressed the uncertainties that laboratory measurements presented, especially the abnormally high values of the dielectric constant at low frequencies, which could be caused by measurement artifacts, such as polarization effects at the sample-electrode interface. In a subsequent study, Scott (1983) expanded upon this foundational work by providing refined analyses of permittivity in the low-frequency regime and conductivity at higher frequencies. Furthermore, this research extended the scope of investigation to horizontally stratified media, detailing the application of the Wenner method to characterize the resistivity profiles of distinct layers within both soil and rock formations.

Longmire *et al.* (1975) utilized experimental data from Scott (1964) and Wilkenfeld *et al.* to derive a soil impedance model that explicitly accounts for frequency-dependent constitutive parameters. The fundamental premise of their approach is that the soil medium can be represented by an equivalent network of resistors and capacitors, thereby defining the constitutive relationship between current density ($\mathbf{J}$) and electric field ($\mathbf{E}$). Consequently, the macroscopic impedance and admittance are characterized by the summation of these resistive and capacitive elements. Analytically, this formulation demonstrates that soil permittivity is inversely proportional to frequency, whereas conductivity exhibits a direct proportionality. Furthermore, the proposed model correlates soil moisture content—based on Scott's datasets with dielectric loss, employing a curve-fitting extrapolation technique to characterize the soil's attenuation profile.

2.2 EXISTING ANALYTICAL FORMULATION

Carson (1926) and Pollaczek (1926) established the theoretical foundation for the analysis of overhead transmission lines with earth return. Pollaczek provided the rigorous integral solution to the problem of a conductor above a lossy half-space. However, it was Carson who introduced the widely adopted formulation by deriving a tractable series approximation for the self and mutual impedances. Carson's model relies on the magnetoquasistatic pure assumption, treating the soil as a homogeneous medium with constant conductivity and neglecting displacement currents—an approximation valid primarily at low frequencies.

Wise *et al.* (1934) extended the work of Carson and Pollaczek to higher frequencies. Wise derived expressions for earth return impedance and potential coefficients that explicitly incorporate the finite permittivity of the soil. This contribution was pivotal for modeling high-frequency phenomena, where displacement currents in the ground become significant and can no longer be neglected. By including the soil's dielectric constant, Wise generalized the calculation of earth return impedance and admittance, allowing for a more precise representation of electromagnetic wave propagation in dispersive media.

Nakagawa *et al.* (1976) advanced transmission line modeling by developing a generalized formulation for earth return impedance in vertically stratified soil (N-layers). This approach provides a realistic representation of geological structures by accounting for multiple layers with distinct electrical properties. Furthermore, in 1981, Nakagawa refined Wise's earlier work, placing specific emphasis on the accurate inclusion of displacement currents in the calculation of shunt admittance.

H. Xue *et al.* (2018) systematically compared constant-parameter models against frequency-dependent approaches. Their findings confirmed that considering soil dispersion leads to a significant reduction in calculated lightning-induced overvoltages. Additionally, Xue proposed the "Extended Transmission Line" (ETL) concept to address the mode transition from quasi-TEM to surface wave propagation. Grounded in Wise's analytical formulations, the ETL approach effectively characterizes high-frequency transients (up to 100 MHz) in gas-insulated buses and overhead lines.

T. A. Papadopoulos *et al.* (2021) focused on the integration of frequency-dependent soil models into time-domain simulations. Their work underscores the necessity of considering the dispersive nature of soil for the accurate determination of modal propagation characteristics and transient overvoltages. Papadopoulos developed methodologies to incorporate experimental soil formulations—such as the Visacro-Alípio model—into rational approximation routines like the Universal Line Model (ULM). These studies demonstrated that neglecting frequency dependence significantly compromises the realism of high-frequency simulations, particularly those involving lightning-induced phenomena.

Martins-Britto *et al.* (2024) applied advanced electromagnetic modeling to the analysis of transient interference between spatially coupled systems, such as overhead transmission lines

and underground pipelines. Their contribution provides rigorously derived expressions to quantify the mutual capacitive coupling mechanisms in these hybrid environments, addressing the complex interaction between aerial and buried conductors.

2.3 VERTICAL LAYERS

An exhaustive literature search confirmed a notable scarcity of research applying vertically layered soil models to the calculation of transmission line parameters. While tangentially related work exists, it does not address the central problem of the calculation Z and Y. For instance, a study in (ŞTEţ *et al.*, 2012) evaluated an EMI problem involving a pipeline in a vertically layered soil but did not focus on the calculation or use of the corresponding line parameters. Another work (JIANG *et al.*, 2023) proposed a new formulation based on coordinate transformation to analyze how vertically layered soil affects lightning return stroke propagation, concluding that the vertical electric field is significantly influenced, but it did not address transmission line parameters. In contrast to this gap, the modeling of grounding systems in vertically stratified soils is a well-established field with numerous publications (HUANG *et al.*, 2014; ZENG *et al.*, 2004; LI *et al.*, 2007; BATISTA; PAULINO, 2021; NAYEL, 2014a; NAYEL *et al.*, 2012; NAYEL, 2014b). This disparity highlights the novelty and importance of the present research.

Like it was said, accurate soil modeling is fundamental for the realistic calculation of transmission line parameters. As previously discussed, established models typically assume homogeneous or horizontally stratified configurations. While useful, these approaches fail to capture the geological complexity of many real-world regions where abrupt lateral transitions in subsoil composition and resistivity (ρ) occur.

The absence of direct references for vertically stratified transmission line models presents a significant challenge for the validation of the results obtained in this work. As will be detailed in the following chapters, the validation relies on cross-verification between the proposed method and simulations performed with well-established tools, such as the Finite Element Method Magnetics (FEMM) software and the `LineCableLab` toolbox (MARTINS-BRITTO *et al.*, 2023), which have been previously validated for a wide range of electromagnetic problems.

2.4 CHAPTER SUMMARY

This chapter provided the theoretical and bibliographic foundation for the thesis. It began by introducing the fundamentals of transmission line parameters (series impedance (Z) and shunt admittance Y) and established their critical dependence on complex soil properties, including heterogeneity and frequency dependence. A literature review the evolution of soil modeling, highlighting that existing research and commercial software have focused almost exclusively on homogeneous or horizontally layered soils. The central conclusion of this review is the identification of a significant research gap: the rigorous calculation of transmission line parameters in vertically stratified soil models remains unaddressed. This chapter thus establishes the novelty of the present work and the validation challenges (the absence of real data) that subsequent chapters must overcome.

Table 2.1 shows the summary the advantages and disadvantages of each formulation or model. The k_x columns is to respect of the naturally calculation of the longitudinal propagation constant in the formulation.

Table 2.1. Comparison of Earth Return Formulations.

Formulations	**Horiz. Multi-layer**	**Freq. Dep. Soil**	**Disp. Current**	**Soil Permittivity**	**Valid up to 1 MHz**	**Vertical Multi-layer**	**k_x**
Carson and Pollaczek	✗	✗	✗	✗	✗	✗	✗
Wise	✗	✗	✓	✓	✓	✗	✗
Nakagawa	✓	✗	✓	✓	✗	✗	✗
Xue	✓	✓	✓	✓	✓	✗	✗
Papadopoulos	✓	✓	✓	✓	✓	✗	✗
Martins	✓	✓	✓	✓	✓	✗	✗
Proposed Model	✓	✓	✓	✓	✓	✓	✓

CHAPTER 3

THEORICAL FOUNDATION

This chapter delineates the computational based on the FEM and establishes the analytical benchmark employed for model verification.

The primary contribution present in this chapter, lies in the advancement of the FEM modeling capabilities. To calculate the line parameters, the `LineCableLab` toolbox (MARTINS-BRITTO *et al.*, 2023) was utilized and extended, specifically through geometric modifications required to simulate vertically stratified soil layers.

Furthermore, the analytical formulation that underpins the analysis in subsequent chapters is detailed herein. The Martins-Papadopoulos-Chrysochos formalism is presented, providing the rigorous analytical derivations necessary to model the capacitive coupling between overhead transmission lines and buried pipelines.

3.1 ANALYTICAL EARTH IMPEDANCES FOR HOMOGENEOUS SOIL

This section introduces the analytical benchmark used to validate the proposed FEM formulations. A robust verification is essential because the FEM models will later be applied to complex vertically layered soils, a geometry for which no closed-form analytical solution exists. While numerous analytical models for underground systems are available (MAGALHãES *et al.*, 2015; XUE *et al.*, 2018b; PAPADOPOULOS *et al.*, 2011; PAPADOPOULOS *et al.*, 2010), a benchmark with high precision is required.

While many foundational models rely on magnetoquasistatic, which are a intermediate simplification of Maxwell equations between static and high frequency, assumptions that neglect displacement currents—thereby limiting their accuracy at higher frequencies—the formulation proposed by Martins-Papadopoulos-Chrysochos (MARTINS-BRITTO *et al.*, 2024) offers a rigorous alternative. This model was selected as the primary benchmark because it explicitly

accounts for displacement currents, frequency-dependent soil parameters, and the dielectric properties of both the air and soil half-spaces. Furthermore, it is applicable to hybrid conductor configurations (i.e., overhead and underground) and remains valid for frequencies up to 1 MHz.

Notably, this analytical formulation is derived from the Helmholtz equation, which inherently captures wave propagation phenomena by retaining the displacement current terms. This stands in distinct contrast to the Baseline FEMM formulation presented in the next section, which relies on the magnetoquasistatic diffusion equation.

However, a critical theoretical distinction must be noted: the analytical benchmark operates under the assumption of a zero longitudinal propagation constant ($k_x = 0$) (MARTINS-BRITTO *et al.*, 2024, Section III) as shown in Eq.3.9. In contrast, the Enhanced formulation proposed in this work (shown in the following chapter) derived directly from Maxwell's equations (under the Darwin approximation (DARWIN, 1920)), allowing the propagation characteristics to be modeled inherently without this restrictive assumption. Consequently, discrepancies between the proposed formulation and the analytical benchmark are expected, attributable to the fundamental theoretical distinction regarding the longitudinal propagation constant (k_x). It is pertinent to acknowledge that experimental validation for these complex, vertically stratified scenarios remains an open challenge; to the best of the authors' knowledge, high-fidelity measurement data suitable for corroborating these specific high-frequency findings is currently absent from the literature.

In the following, this analytical formula for homogeneous soil will be used to compute the reference parameters. These results will serve as the references to quantify the accuracy of the new FEM models when they are applied to an identical homogeneous case. Following this references, the physical consistency of the vertically layered FEM model will be assessed by comparing the results of the two-layer model against two uniform limiting cases (representing ρ_1 and ρ_2), with the expectation that the vertical model's impedance will be physically situated between these two uniform extremes. The impedance and potential for conductors i and j in the air medium (with height $h_i, h_j > 0$) is present in Eq. (3.1):

$$Z_{eij}^{00} = \frac{j\omega\mu_0}{2\pi} \int_0^\infty F^0(\lambda) \cos(\lambda y_{ij})\, d\lambda \tag{3.1}$$

$$F^0(\lambda) = \frac{e^{-a_0 H_{ij}} - e^{-a_0 H_{ij}}}{a_0} + \frac{2\mu_1 e^{-a_0 H_{ij}}}{(a_0\mu_1 + a_1\mu_0)} \tag{3.2}$$

$$P^{00}_{eij} = \frac{j\omega}{2\pi(\sigma_0 + j\omega\varepsilon_0)} \times \int_0^\infty \left[F^0(\lambda) + G^0(\lambda)\right] \cos(\lambda y_{ij})\, d\lambda \tag{3.3}$$

$$G^0(\lambda) = -\frac{2\mu_0\mu_1 a_0(\gamma_1^2 - \gamma_0^2)e^{-a_0 H_{ij}}}{(a_0\mu_0\gamma_1^2 + a_1\mu_1\gamma_0^2)(a_0\mu_1 + a_1\mu_0)} \tag{3.4}$$

For the calculation of the impedance and admittance in the soil medium Eq.3.5 is employed for conductors i and j in the soil medium (for a depth of $h_i, h_j < 0$):

$$Z^{11}_{eij} = \frac{j\omega\mu_1}{2\pi} \int_0^\infty F^1(\lambda) \cos(\lambda y_{ij})\, d\lambda \tag{3.5}$$

$$F^1(\lambda) = \frac{e^{-a_1 H_{ij}} - e^{+a_1 H_{ij}}}{a_1} + \frac{2\mu_0 e^{+a_1 H_{ij}}}{(a_0\mu_1 + a_1\mu_0)} \tag{3.6}$$

$$P^{11}_{eij} = \frac{j\omega}{2\pi(\sigma_1 + j\omega\varepsilon_1)} \times \int_0^\infty \left[F^1(\lambda) + G^1(\lambda)\right] \cos(\lambda y_{ij})\, d\lambda \tag{3.7}$$

$$G^1(\lambda) = \frac{2\mu_0\mu_1 a_1(\gamma_0^2 - \gamma_1^2)e^{+a_1 H_{ij}}}{(a_1\mu_1\gamma_0^2 + a_0\mu_0\gamma_1^2)(a_0\mu_1 + a_1\mu_0)} \tag{3.8}$$

with

$$a_k = \sqrt{\lambda^2 + \gamma_k^2 + k_x^2}, \quad \overline{H_{ij}} = |h_i - h_j|, \quad H_{ij} = (h_i + h_j). \tag{3.9}$$

The self-quantities are obtained from (3.1) (3.5) by setting $h_i = h_j$ and by equating y_{ij} to the external radius of the corresponding conductor. $F^k(\lambda)$ is the modified spatial frequency Fourier transform of the medium k with respect to λ.

For conductors in different medium the Eq.3.10 and Eq.3.11 is used.

$$Z^{mn}_{eij} = Z^{nm}_{eij} = \frac{j\omega\mu_0\mu_1}{\pi} \int_0^\infty \frac{e^{(-a_0 h_i + a_i h_j)}}{a_0\mu_i + a_1\mu_0} \cos\lambda y_{ij} d\lambda \tag{3.10}$$

$$\begin{gathered} P^{mn}_{eij} = P^{nm}_{eij} = \frac{-\omega^2\mu_0\mu_1}{\pi} \times \\ \int_0^\infty \frac{(a_0\mu_0 + a_1\mu_1)e^{-a_0 h_i + a_1 h_j}}{(a_1\mu_1\gamma_0^2 + a_0\mu_0\gamma_1^2)(a_0\mu_1 + a_1\mu_0)} \end{gathered} \tag{3.11}$$

In these equations, the superscripts in Z^{mn} and P^{mn} indicate the media in which the source conductor (m) and the observation conductor (n) are located, respectively. The index $k = 0$ corresponds to the upper medium (air), while $k = 1$ refers to the lower medium (soil). The variable λ is the integration variable of the inverse Fourier transform. This formulation is already implement in `LineCableLab` (MARTINS-BRITTO *et al.*, 2023).

The electromagnetic properties of air—permittivity, permeability, and conductivity—are denoted by ε_0, μ_0, and σ_0, respectively. Similarly, the corresponding parameters for the soil are ε_1, μ_1, and σ_1. The propagation constant for each medium is defined as:

$$\gamma_k = \sqrt{j\omega\mu_k(\sigma_k + j\omega\varepsilon_k)}, \quad k \in \{0, 1\} \tag{3.12}$$

where ω is the angular frequency.

For the admittance an operation is made using the Maxwell potentials $\mathbf{P}$, and is shown in Eq. 3.13.

$$\begin{aligned}\mathbf{Y} = j\omega\mathbf{P}^{-1} &= j\omega \begin{bmatrix} P_{self,ov} & P_{mut,ov-und} \\ P_{mut,ov-und} & P_{self,und} \end{bmatrix}^{-1} \\ &= \frac{j\omega}{P_{self,und}P_{self,ov} - P^2_{mut,ov-und}} \begin{bmatrix} P_{self,und} & -P_{mut,ov-und} \\ -P_{mut,ov-und} & P_{self,ov} \end{bmatrix},\end{aligned} \tag{3.13}$$

so:

$$Y_{mut,ov-und} = -j\omega \frac{P_{mut,ov-und}}{P_{self,und}P_{self,ov} - P^2_{mut,ov-und}}, \tag{3.14}$$

in which subscript "ov" denotes the overhead conductor and "und" denotes the underground pipeline. The computation of the mutual admittance depends on the self-potential term defined in Eq. (3.6). This expression exhibits an inherent mathematical singularity when the conductor heights are identical ($h_i = h_j$), causing the term H_{ij} to vanish. To mitigate this numerical instability, the implementation utilizes a regularization technique, introducing a negligible perturbation to the distance parameter to prevent singularity convergence. While ongoing research aims to resolve this integral analytically using Bessel functions, the current numerical approximation provides sufficient accuracy for the verification purposes of this study, without compromising the validity of the benchmark.

3.2 BASELINE QUASI-STATIC FEM FORMULATION

This section introduces a method using the solver FEMM (MEEKER, 2020) to account for lateral variations in soil resistivity in earth-return impedance and admittance calculations, improving model accuracy under steady-state EMI simulations. Three cases are examined: homogeneous soils with resistivity values of 100 Ω-m and 1000 Ω-m, and a vertically stratified

soil case with 100/1000 Ω-m. The FEM-derived mutual impedances are then applied to predict induced voltages in an underground pipeline near a 150 kV single-circuit overhead line.

To simulate the system in FEMM, the `LineCableLab` toolbox in MATLAB, available in (MARTINS-BRITTO *et al.*, 2023) was used. In addition to assembling the system, the toolbox runs the FEM frequency-scan and collects the self- and mutual-impedances and admittances, providing comparisons with several analytical models (Carson, Pollaczek, Wise, Papadopoulos) that are chosen by the user. Additional codes were incorporated to the original toolbox code, to allow for simulations with N vertical layers.

In the formulations presented below, the dimensions of the computational domain are scaled according to the electromagnetic skin depth (δ) of the soil. This ensures that the domain is sufficiently large for the fields to decay to negligible values at the boundaries. For the baseline formulation, the domain truncation boundaries range from 5000 m to 10000 m, governed by the skin depth equation:

$$\delta = \sqrt{\frac{\rho}{\pi f \mu}} \tag{3.15}$$

where ρ is the soil resistivity, f is the frequency, and μ is the magnetic permeability.

3.2.1 FEMM Formulation and Governing Equations

The adopted FEM formulation is a low-frequency approximation in a 2D plane configuration. Therefore, the system impedances and admittances are calculated as part of the decomposed time-harmonic magnetic and quasi-electrostatic problems, respectively. For both problems, the FEMM software, as documented in Meeker (2020), is applied. The entire simulation workflow is automated through MATLAB scripts, provided by Meeker (2020), which create the geometry, add material properties, run the solver, and extract the results into FEMM. This interaction is accomplished by sending commands written in Lua, the native extension language integrated into FEMM to enable scripting and batch processing capabilities.

3.2.1.1 Magnetics problem

For the Series impedance, the Time-Harmonic Magnetic Problems module is used in FEMM. The formulation describe in (MEEKER, 2020) begins by defining the current density as:

$$\mathbf{J} = \sigma \mathbf{E} \tag{3.16}$$

Which σ is the electric conductivity. The induced electric field then obeys:

$$\nabla \times \mathbf{E} = -\dot{\mathbf{B}} \tag{3.17}$$

Substituting the vector potential form of $\mathbf{B}$ into (3.17) yields:

$$\nabla \times \mathbf{E} = -\nabla \times \dot{\mathbf{A}} \tag{3.18}$$

where the $\mathbf{A}$ is the magnetic vector potential. In the case of 2-D problems:

$$\mathbf{E} = -\dot{\mathbf{A}} - \nabla V \tag{1.11}$$

and the constitutive relationship:

$$\mathbf{J} = -\sigma \dot{\mathbf{A}} - \sigma \nabla V \tag{3.19}$$

As can be seen from Eq.(3.19), for time-varying magnetic problems, the FEMM solver use a simplified form of Maxwell's equations that neglects displacement current. This approach is adopted because the software is specifically designed for low-frequency applications (MEEKER, 2020). The same formulation has been also used in a number of relevant papers (TSIAMITROS *et al.*, 2006) for the case of overhead underground systems and (TRIANTAFYLLIDIS *et al.*, 1999) for overhead conductors. In fact, (TRIANTAFYLLIDIS *et al.*, 1999) describes the theoretical background of the FEM modelling used in (TSIAMITROS *et al.*, 2006).

The mutual complex impedance Z_{ij} is extracted by setting a magnetic problem and imposing a 1 A current to the source conductor i, zero to the target conductor j, and measuring the V_i voltage drop, as expressed in (3.20). The self-impedance can also be calculated using (3.20), making $i = j$ (PAPAGIANNIS *et al.*, 2005).

$$Z_{ij} = \frac{V_i}{I_j} \quad (i,j = 1, 2, ...n) \tag{3.20}$$

The voltage V_i is computed using the block integral of the cross-sectional area S and the magnetic vector potential $\vec{A}$ (MEEKER, 2020). The procedure involves calculating the cross-sectional area S with the block integral function, and the magnetic vector potential $\vec{A}$ is obtained by dividing the block integral of the potential by the cross-sectional area S, representing the integral of the current over the surface S. The resulting current density J is then computed using the (3.21).

$$J = j\omega\sigma_i\vec{A} \tag{3.21}$$

where σ_i is the conductivity from conductor i.

The complete formulation for the impedance is shown in (3.22).

$$Z_{ij} = \frac{V_i}{I_j} = \frac{J_{szi}/\sigma_i}{I_j} \quad [\Omega/m] \tag{3.22}$$

in which Z_{ik} is the mutual impedance between conductor i and conductor k, J_{szi} is the current density generated in the $\hat{z}$ direction for conductor i, and σ_i is the conductivity of conductor i.

3.2.1.2 Electrostatic Problems

The shunt admittance calculation in FEMM is based on solving the electrostatic problem. This is governed by Gauss's Law ($\nabla \cdot D = \rho$) and the irrotational property of the E-field ($\nabla \times E = 0$), with the software assuming a linear constitutive relationship ($D = \varepsilon E$).To simplify the computation, the electric field is defined using the electric scalar potential, V, through the relationship:

$$E = -\nabla V$$

This definition automatically satisfies the irrotational condition ($\nabla \times E = 0$). When substituted into Gauss's Law, this yields the final governing partial differential equation for regions of homogeneous permittivity, which is Poisson's equation:

$$-\varepsilon\nabla^2 V = \rho$$

FEMM solves this equation for the potential V over the user-defined domain, sources, and boundary conditions.

To extract the earth-return admittance, the source conductor is energized with 1 V, and the target conductor is kept at 0 V. The admittance is obtained by calculating the line inte-

gral of the displacement field normal to the conductor external circumference, as described in (3.23) (MEEKER, 2020):

$$\int_C \vec{D}.\hat{n} \tag{3.23}$$

3.3 CHAPTER SUMMARY

This chapter established the theoretical and computational foundations employed in this study for the determination of earth return parameters. The investigation relies on two distinct modeling formulations: a rigorous analytical benchmark and a baseline FEM formulation.

The analytical formulation proposed by Martins, Papadopoulos, and Chrysochos (MARTINS-BRITTO *et al.*, 2024) was selected for the purpose of verifying the other FEM formulations. This choice is justified by the formulation's rigorous inclusion of displacement currents and its capability to model hybrid overhead-underground configurations. However, the application of this method is fundamentally restricted to homogeneous media. Furthermore, the numerical evaluation of the governing improper integrals poses significant computational challenges. The integration kernels can lead to slow convergence or numerical instability, particularly when resolving complex conductor geometries, high-frequency interactions, and lower soil resistivities.

Conversely, the computational workflow utilizing the FEMM solver (MEEKER, 2020) and the `LineCableLab` toolbox (MARTINS-BRITTO *et al.*, 2023) provides the necessary flexibility to handle lateral soil heterogeneities. This baseline approach relies on a decoupled field analysis, solving a magnetoquasistatic problem for series impedance and an electrostatic problem for shunt admittance. While effective for steady-state analysis, this formulation is constrained by the magnetoquasistatic assumption, which neglects the contribution of displacement currents in the magnetic diffusion equation that is significant at higher frequencies.

This approximation limits the accuracy of the baseline FEM model to low-frequency regimes. Consequently, the inability of the baseline solver to fully capture high-frequency phenomena motivates the development of the **Enhanced Formulation**. This approach is designed to address these physical omissions and extend the validity of the model into high-frequency spectrum.

CHAPTER 4

ENHANCED FEM FORMULATION

To address the fundamental limitations of the baseline formulation presented in Section 3.2, this chapter introduces the Enhanced FEM. This advanced numerical model is implemented utilizing the `GetDP` (GEUZAINE, 2007). The solver is integrated into a modern, open-source toolchain orchestrated via the Julia programming language, a platform selected for its high-performance computing capabilities and robust scientific ecosystem.

The Enhanced FEM formulation constitutes the core computational engine of the toolbox `LineCableModels.jl` (MARTINS, 2025), a versatile package designed for the comprehensive modeling of transmission line and cable systems. This environment facilitates the detailed representation of conductors and insulation layers while managing the calculation of frequency-dependent line constants. For the numerical field solution, the toolbox interfaces with the `GetDP` solver and the `Gmsh` mesh generator (GEUZAINE *et al.*, 2009) via the Julia wrappers `GetDP.jl` (MARTINS; LESSA, 2025) and Gmsh (GEUZAINE *et al.*, 2009).

A distinct contribution of this work is the development of the high-level integration layer provided by `GetDP.jl` (MARTINS; LESSA, 2025). This API enables the programmatic construction of the simulation by defining all necessary components—such as function spaces, weak formulations, and resolution procedures—directly within the Julia environment. This architecture ensures a fully automated and reproducible workflow for solving complex electrodynamic problems.

A defining feature of `GetDP` is its symbolic approach to physics definition. Unlike rigid solvers such as FEMM, where the governing equations are pre-compiled and immutable, `GetDP` requires the user to explicitly define the partial differential equations via its proprietary script syntax. While this architecture demands a more rigorous definition of the problem state, it affords a level of modeling flexibility and precision unattainable in standard "black-box" software.

The following sections detail the two critical components of this custom implementation:

first, the rigorous derivation of the governing equations, and second, the Shell Domain Transformation, a boundary technique implemented to correctly model the asymptotic behavior of fields in unbounded regions.

4.1 GETDP FORMULATION AND GOVERNING EQUATIONS

The formulation detailed in this section addresses the inherent limitations and simplifying assumptions of the baseline model presented in the previous chapter. By incorporating the relevant constitutive terms previously neglected, this approach provides a more rigorous representation of the underlying physical phenomena. Furthermore, the open boundary problem is resolved through the implementation of an infinity transformation (shell mapping), which enforces the correct asymptotic decay of the electromagnetic fields. Consequently, the resulting parameters are expected to diverge from the baseline predictions, yielding a higher degree of physical fidelity.

Regarding the computational domain, the sizing strategy remains governed by the skin depth criterion defined in Eq. 3.15. However, the truncation limits have been refined to a range of 500 m to 5000 m. This reduction is necessitated by the significantly higher mesh density required by the Enhanced formulation; maintaining the expansive domain of the baseline model would incur a prohibitive computational cost.

4.1.1 Magneto quasi-static with Darwin's terms formulation

The impedance calculation begins with Ampère's law in the frequency domain.

$$\frac{1}{\mu}\nabla \times \mathbf{B} = \mathbf{J} \tag{4.1}$$

To solve the problem in terms of potentials, the magnetic vector potential, $\mathbf{A}$, and the electric scalar potential, V, are introduced. The representation of the magnetic field using $\mathbf{A}$ are:

$$\mathbf{B} = \nabla \times \mathbf{A} \tag{4.2}$$

For the electric field the representation is expressed with scalar potential and vector potential:

$$\mathbf{E} = -\nabla V - j\omega\mathbf{A} \tag{4.3}$$

The two term in $\mathbf{E}$ in Eq.(4.3) have the transverse (solenoid) component $-j\omega\mathbf{A}$ and the longitudinal (irrotational) component $-\nabla V$ from charge distributions.

In a fully three-dimensional analysis, electromagnetic field components along all axes are intrinsically coupled. However, the dimensional reduction to a 2D cross-section can obscure these interactions, effectively suppressing the out-of-plane components that mediate full-wave coupling. Standard magnetoquasistatic approximations exacerbate this by neglecting displacement currents entirely. The Darwin formulation (DARWIN, 1920) rectifies this by explicitly retaining the irrotational term $(-\nabla V)$ in the constitutive equations (LARSSON, 2007). By reintroducing this specific component of the electric field, the formulation recovers, partially, the critical capacitive coupling effects acting on the planar fields—effects that would otherwise be lost in the dimensional reduction—thereby significantly broadening the physical scope of the simulation beyond the strict quasi-static limit.

The current density can be expressed as:

$$\mathbf{J} = (\sigma + j\omega\varepsilon)\mathbf{E} \tag{4.4}$$

In this form, $\mathbf{J}$ contains both the conduction and displacement current components. By expressing the magnetic field ($\mathbf{B}$) and the current density ($\mathbf{J}$) as functions of the potentials, Ampère's law can be reformulated into a governing differential equation for $\mathbf{A}$.

$$\frac{1}{\mu}\nabla \times \nabla \times \mathbf{A} = -(\sigma + j\omega\varepsilon)\nabla V - (j\omega\alpha - \omega^2\varepsilon)\mathbf{A} \tag{4.5}$$

Under magnetoquasistatic conditions ($\nabla \cdot \mathbf{A} = 0$), and using the vector identity $\nabla \times \nabla \times \mathbf{A} = \nabla(\nabla \cdot \mathbf{A}) - \nabla^2\mathbf{A}$, the equation takes the form:

$$-\frac{1}{\mu}\nabla^2\mathbf{A} + (j\omega\sigma - \omega^2\varepsilon)\mathbf{A} = -(\sigma + j\omega\varepsilon)\nabla V \tag{4.6}$$

Knowing that the source current density associated with the scalar potential gradient is:

$$\mathbf{J}_s = -(\sigma + j\omega\varepsilon)\nabla V \tag{4.7}$$

This source current density is assumed constant over the cross-section of a conductor. Consequently the Eq. 4.8.

$$-\frac{1}{\mu}\nabla^2\mathbf{A} - (j\omega\sigma - \omega^2\varepsilon)\mathbf{A} + \mathbf{J}_s = 0 \tag{4.8}$$

It can be concluded that the total current density is:

$$\mathbf{J} = -(j\omega\sigma - \omega^2\varepsilon)\mathbf{A} + \mathbf{J}_s \tag{4.9}$$

By integrating the total current density across the cross-sectional area S_c, we obtain the current I:

$$I = \int_{S_c} \mathbf{J}\, dS \tag{4.10}$$

Therefore, the mutual impedance Z_{ij} is given by:

$$Z_{ij} = \frac{V_i}{I_j} \tag{4.11}$$

Where I_j is the current injected into the j-th conductor and V_i is the measured voltage on the i-th conductor. In the utilized formulation, Eqs. (4.9) and (4.10) are already implemented using the Galerkin method in `GetDP` to obtain the self and mutual impedances.

4.1.2 Electrodynamics formulation

For the admittance calculation, the formulation begins with the continuity equation, assuming there is no volume charge density:

$$\nabla \cdot \mathbf{J} = 0 \tag{4.12}$$

Using (4.4) and substituting $\mathbf{E} = -\nabla V$, we have:

$$(\sigma + j\omega\varepsilon)\nabla^2 V = 0 \tag{4.13}$$

The method in this formulation to extract the admittance is adding 1 V in a conductor and collect the charge in the other conductors as expressed in Eq.4.14.

$$Y_{ij} = \frac{q_j}{V_0} \tag{4.14}$$

The charge q_j on the j-th conductor is calculated by:

$$q_j = \oint_{\Gamma_{cj}} \mathbf{D} \cdot d\mathbf{l} \tag{4.15}$$

Where $\mathbf{D}$ is the electric displacement field and Γ_{cj} represents the boundary of the cross-section of the j-th conductor. In the formulation, it is (4.12) that is implemented, also via the Galerkin method in `GetDP`.

It is important to note that the physical meaning of the scalar potential V is distinct in the impedance and admittance formulations. For the impedance calculation, V represents the longitudinal voltage drop resulting from the current I_j. For the admittance calculation, it represents the transverse potential applied to the conductors.

4.2 BOUNDARY TRANSFORMATION

A well-known challenge in applying the Finite Element method to electromagnetism is the modeling of unbounded, open-region problems. Since electric and magnetic fields naturally extend to infinity, they must be mathematically mapped onto a finite, discretized domain for numerical analysis. One established technique to address this is the shell domain transformation, a form of infinite domain mapping (HENROTTE *et al.*, 1999; IMHOFF *et al.*, 1990).

This principle involves a coordinate transformation that maps the infinite exterior domain onto a finite "shell" region, which is bounded by two surfaces: An inner artificial boundary that encloses the primary domain of interest, and an outer boundary that mathematically represents infinity.

The concept of the shell transformation is illustrated in Figure 4.1. A boundary condition, such as a **Dirichlet boundary condition** (e.g., setting the potential to a fixed value of zero), can then be applied directly to this outer boundary to correctly model the field behavior at infinity.

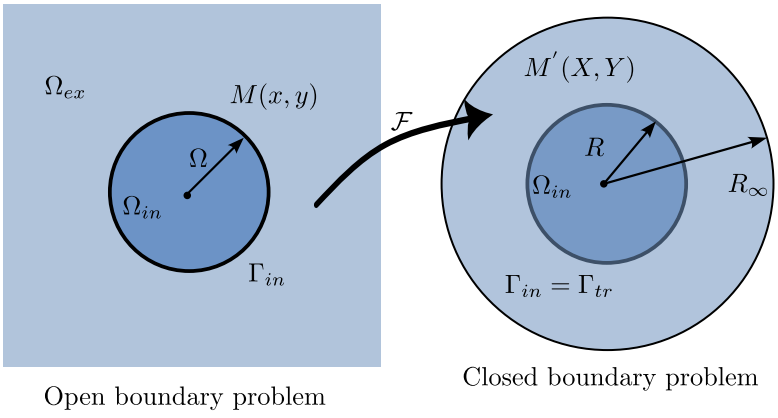

Figure 4.1. Illustration of the infinite shell transformation. Adapted from (IMHOFF *et al.*, 1990).

This technique offers significant advantages (FREEMAN; LOWTHER, 1989). It allows the field to be calculated at all points in space, and the external field can be recovered through a

inverse transformation. Furthermore, modeling the exterior region with a finite element mesh produces a sparse coefficient matrix, which is highly beneficial as it permits the use of efficient sparse matrix solvers (FREEMAN; LOWTHER, 1989).

This transformation is directly supported by the `GetDP` solver through the built-in " VolSphShell " function, which computes the Jacobian for the volume transformation (GEUZAINE, 2007). The function's usage is described below.

4.3 COMPARATIVE FORMULATION ANALYSIS

For the Series Impedance, the key difference is that the simplified version neglects the displacement current, which leaves it inaccurate for high frequencies and only presents the conductive component, unlike the enhanced model. Furthermore, the enhanced model has the shell transformation that solves the problem of open-region.

As previously delineated, the Enhanced formulation is rigorously derived from Maxwell's equations, thereby implicitly capturing the longitudinal propagation constant. This stands in fundamental contrast to the Baseline FEMM formulation, which is constrained by the magneto-quasistatic assumption. Consequently, two primary theoretical distinctions drive the observed divergence in the results: the rigorous inclusion of displacement currents and the inherent modeling of wave propagation effects.

Table 4.1: Comparison of Formulations: Series Impedance (Magnetic Problem).

Simplified (Baseline)	**Enhanced Formulation**
Assumes displacement current is negligible.	Accounts for both conduction and displacement currents.
Current density is defined by conduction only: $\mathbf{J} = \sigma\mathbf{E}$	Current density includes both terms: $\mathbf{J} = (\sigma + j\omega\varepsilon)\mathbf{E}$
The resulting formulation neglects permittivity (ε): $\mathbf{J} = -\sigma\dot{\mathbf{A}} - \sigma\nabla V$	The resulting formulation retains permittivity (ε): $\mathbf{J} = -(j\omega\sigma - \omega^2\varepsilon)A - (\sigma + j\omega\varepsilon))V$

The first formulation represents the electrostatic case, derived from the divergence form of Ampère's law under static conditions (ignoring time-varying fields), where the electric field $\mathbf{E}$ is purely conservative ($\mathbf{E} = -\nabla V$). The extraction relies on Gauss's law $\int_C \mathbf{D} \cdot \mathbf{n}\, dS$ to compute

enclosed charge. In contrast, the second formulation is a Electrodynamics formulation, starting from the continuity equation $\nabla \cdot \mathbf{J} = 0$ (assuming steady-state currents with no net charge accumulation), leading to a complex governing equation $(\sigma + j\omega\varepsilon)\nabla^2 V = 0$ that incorporates conductivity σ, angular frequency ω, and permittivity ε, effectively describing diffusion behavior of fields in lossy materials. The extraction method $\oint_S \mathbf{D} \cdot d\mathbf{S}$ similarly applies Gauss's law but accounts for displacement currents in the frequency domain.

Table 4.2: Comparison of Formulations: Shunt Admittance (Electrical Problem).

Simplified (Baseline)	**Enhanced Formulation**
Derived from the divergence of Ampère's Law: $E = -\nabla V$	Starts from the continuity equation (assuming no source): $\nabla \cdot \mathbf{J} = 0$
Governing equation: $-\varepsilon\nabla^2 V - \rho = 0$	Governing equation : $(\sigma + j\omega\varepsilon)\nabla^2 V = 0$
Extraction method: $\int_C \vec{D} \cdot \hat{n}\, dS$	Extraction method: $\oint_S \mathbf{D} \cdot d\mathbf{S}$

4.4 CHAPTER SUMMARY

This chapter detailed the theoretical and computational architecture of the Enhanced FEM formulation, designed to improve the physical approximations of the baseline model. The implementation relies on a high-performance, open-source toolchain orchestrated within the `LineCableModels.jl` toolbox. A distinct contribution is the development of the `GetDP.jl` interface, which enables the programmatic definition of function spaces, formulations, and resolution procedures directly within the Julia environment, ensuring a fully automated and reproducible scientific workflow.

The governing physical equations were rigorously derived for both series impedance and shunt admittance. Unlike the baseline magnetoquasistatic approach, the Enhanced formulation integrates the full complex permittivity term $\sigma + j\omega\varepsilon$ into the Maxwell-Ampère-Darwin and continuity equations. By solving for the magnetic vector potential A and electric scalar potential V, this approach captures both conduction and displacement currents, thereby extending the model's validity range significantly beyond the low-frequency spectrum.

Furthermore, to address the unbounded nature of the electromagnetic fields, the formulation incorporates a shell domain transformation technique. This method mathematically maps the infinite exterior domain onto a finite discretized region, allowing for the rigorous imposition of Dirichlet boundary conditions without the computational penalties or truncation errors associated with simple domain sizing.

Finally, a comparative analysis highlighted the structural differences between the baseline and Enhanced models. The inclusion of displacement currents and the rectification of the open-boundary problem ensure that the Enhanced formulation yields a higher degree of physical fidelity, particularly for high-frequency interactions in complex, vertically stratified soil environments.

CHAPTER 5

RESULTS AND ANALYSIS

This chapter presents three distinct case studies designed to rigorously evaluate the impact of lateral soil stratification on earth return parameters.

First, a fundamental cross-sectional geometry is analyzed to establish a comparative benchmark between the Baseline and Enhanced FEM formulations detailed in previous chapters. This initial case serves to validate the consistency of the numerical methods under controlled conditions.

Second, the analysis is extended to a real-world application scenario. Beyond the calculation of standard transmission line parameters, this case addresses a practical interference situation relevant to the studied configuration. This comparison effectively delineates the operational capabilities and specific validity ranges of both the Baseline and Enhanced formulations.

Third, to demonstrate the robustness of the Enhanced formulation in modeling complex underground infrastructure, a High-Voltage Direct Current (HVDC) system is simulated. This case specifically investigates the influence of lateral soil stratification on the system's transient response. It is important to noted that the Baseline formulation was not use in this case because of the difficulty in creating the cable geometry and the limited formulation.

Crucially, a primary contribution of the Enhanced formulation is its ability to model multi-layered cable systems with high geometric fidelity. Unlike conventional analytical formulations found in the literature—which often rely on simplified representations of cable components (e.g., core, armour, and sheath) or assume massive solid cores—the proposed approach explicitly models the complete cable architecture. This includes the detailed discretization of individual conductor filaments, thereby avoiding the generalizations and potential accuracy discrepancies inherent in simplified analytical models.

5.1 CASE 1

Two uniform cases are evaluated to demonstrate the differences with the vertical soil stratification, with the resistivity of 100, and 1000 Ω-m. The cross-section in Figure 5.1 is used for lateral variation of soil resistivity and homogeneous cases. For the homogeneous case, the properties of soil layer 2 are equal to those of layer 1. The conductors have a resistivity of 1.7×10^{-8} Ω-m, radii of 0.034 m meters and a insulation layer of 0.0266 m.

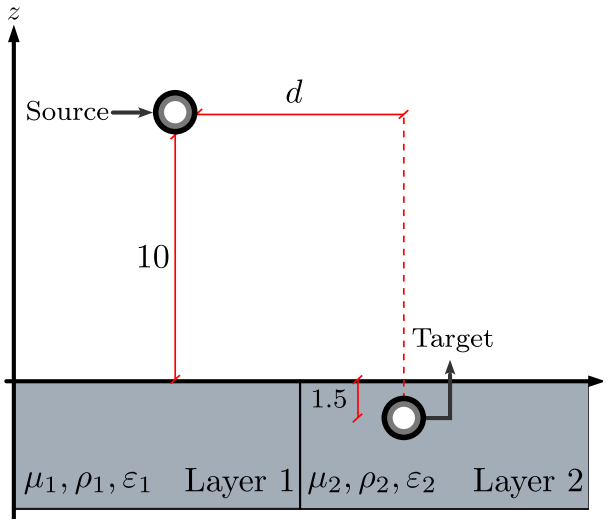

Figure 5.1. Cross-section of the vertically-layered system with two conductors, one overhead and another conductor on the underground with a horizontal distance equal to d.

5.1.1 Baseline formulation

The horizontal distance d is varied from 1 m to 20 m, and the mutual impedance Z_{12} is evaluated at a frequency of 60 Hz. The variations in the horizontal distance d for the three cases are shown in Figure 5.2 for impedance and the admittance in Figure 5.3. The uniform cases are calculated using the Martins-Papadopoulos-Chrysochos.

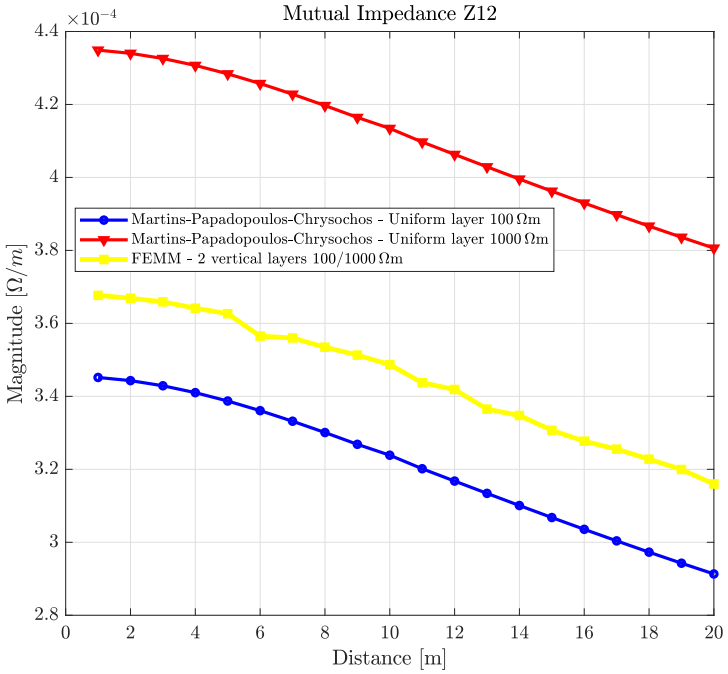

Figure 5.2. Mutual impedance between conductors 1 and 2 versus lateral distance d for vertically-layered and uniform soil models. The source line is in 100 Ω-m layer, and the target line is in 1000 Ω-m layer.

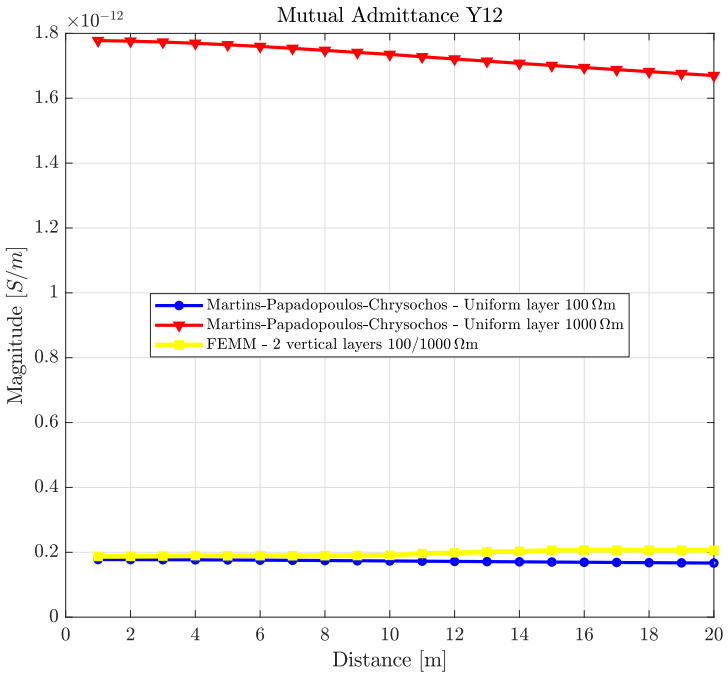

Figure 5.3. Mutual admittance between conductors 1 and 2 versus lateral distance d for vertically-layered and uniform soil models. The source line is in 100 Ω-m layer, and the target line is in 1000 Ω-m layer.

When the vertically stratified soil is approximated by a uniform model ($\rho = 1000\,\Omega$-m), the analysis yields a Root Mean Square Deviation (RMSD) of 19.07%, calculated using Eq. (5.1),

relative to the actual two-layer vertical model. The relationship between induced voltages and mutual impedances, as expressed in (5.2), implies that this overestimation could inflate cost estimates for transmission lines due to the conservative nature of the uniform model. This error might lead engineers to assume that costly mitigation measures are necessary. Moreover, overestimated touch, step voltages, and insulation stresses could falsely indicate higher risks, potentially prompting unnecessary protective actions. Consequences include risks of electric shock, protective coating degradation, equipment damage on underground insulated conductors, and increased corrosion risk (TSIAMITROS *et al.*, 2006).

$$RMSD(\%) = \frac{\sqrt{\frac{1}{n}\sum_{i=1}^{n}\left(Z_{2\text{ layers }100\ 1000,i} - Z_{1000,i}\right)^2}}{\frac{1}{n}\sum_{i=1}^{n} Z_{2\text{ layers }100\ 1000,i}} \times 100 \tag{5.1}$$

$$E = Z_m \times \overline{I}_{TL} \tag{5.2}$$

where i is the horizontal distance between the conductors.

The mutual impedance is calculated in the frequency range of $10 - 100$ Hz for the three soil cases, with results shown in Figure 5.4. In all cases a distance of $d = 1\,m$ was used. The chosen frequency range is justified given the focus on steady-state phenomena in the present study, and the naturally limitation in FEMM solver and formulation. This selection does not constitute any loss of generality, as the proposed approach, based in the physics problem defined by (3.19), i.e. magnetoquasistatic assumption, has been shown to provide reasonable results for frequencies up to the megahertz range (PAPAGIANNIS *et al.*, 2005; MARTINS-BRITTO *et al.*, 2024). In the two-layered model, the mutual impedance stays between the two homogeneous limiting cases ($\rho = 1000\,\Omega$-m and $\rho = 100\,\Omega$-m).

The mutual admittance is also calculated in the same frequency range for the three soil cases, results shown in Figure 5.5. The results produced by this current formulation are physically inconsistent. In contrast to the impedance calculations, which behave as expected, the admittance for the vertically layered soil model does not lie within the interval bounded by the two uniform soil cases ($\rho = 100\ \Omega \cdot$ m and $\rho = 1000\ \Omega \cdot$ m). This limitation is based on the formulation on Section 3.2.1.2.

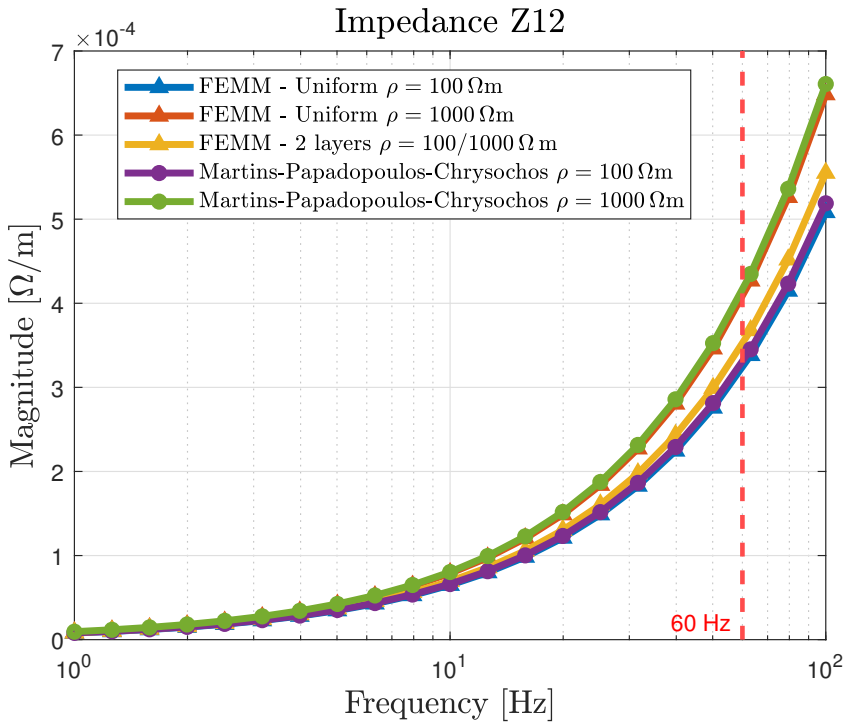

Figure 5.4. Mutual impedance between conductors 1 and 2 for different soil models.

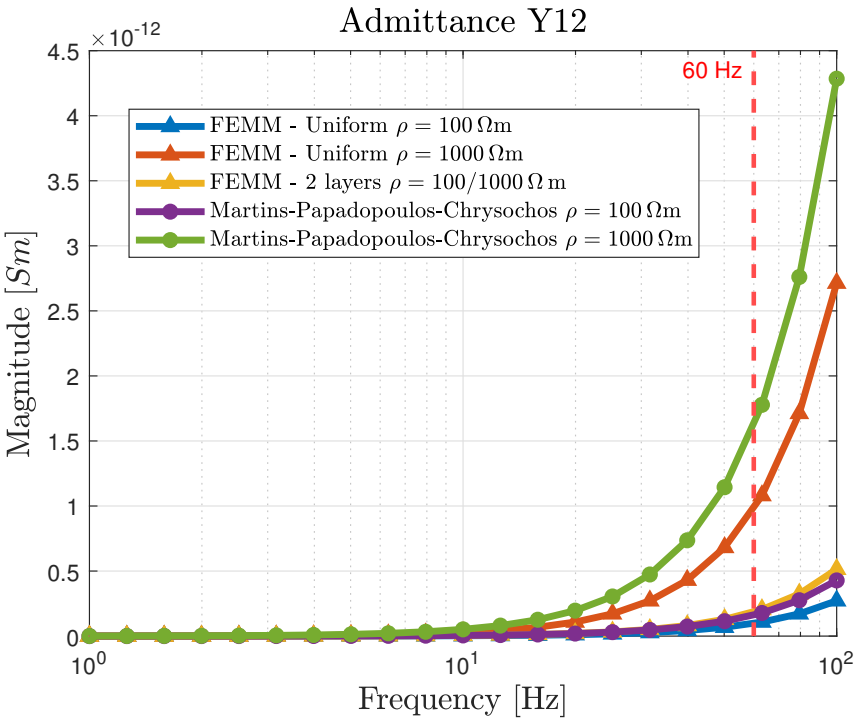

Figure 5.5. Mutual admittance between conductors 1 and 2 for different soil models.

5.1.2 Enhanced formulation

The magnetostatic formulation previously described in Section 3.2.1 neglects the effect of permittivity (ε), which describes the dielectric properties of the materials, and propagation constant (k_x). This omission represents a significant limitation in the model, particularly at higher frequencies. A comparison between the simplified current density in (3.21) and the full expression in (4.9) reveals two critical, frequency-dependent terms that were omitted: the displacement current term ($j\omega\varepsilon$), which accounts for time-varying electric fields in dielectric media, and the wave propagation term ($\omega^2\varepsilon$), which relates to the energy stored in the electric field (i.e., capacitance).

Furthermore, the enhanced formulation presented here computes the admittance matrix by calculating the electric charges on the system's components, an approach analogous to the well-established Method of Maxwell's Potential Coefficients, as shown in (4.14).

To demonstrate the capabilities of this enhanced model, the verification study is revisited. The mutual impedance is calculated for the two-conductor system (Figure 5.1) at a frequency of 60 Hz while varying the horizontal separation distance. Additionally, a wideband frequency sweep, from 0.1 Hz to 1 MHz, is performed for a fixed distance of 1 m. This analysis directly addresses the limitations of the previous magnetostatic model, which failed to produce results consistent with the analytical benchmark model (MARTINS-BRITTO *et al.*, 2024) at high frequencies.

The results presented in Figure 5.6 demonstrate that the enhanced `GetDP` formulation results in a higher mutual impedance value compared to the previous models. This increase is attributed to the more realistic physical modeling, which includes the dielectric and wave propagation effects discussed previously. The uniform soil case with $\rho = 100\ \Omega \cdot \mathrm{m}$, the result from `GetDP` is slightly higher than that of the analytical formulation. However, for the more resistivity soil ($\rho = 1000\ \Omega \cdot \mathrm{m}$), this difference becomes more significant. As expected, the result for the two vertically layered case, when calculated with the new formulation, shows a difference of 8.14%, using (5.1). This discrepancy, which can be highly relevant depending on the application, is explained by the inclusion of the previously neglected permittivity terms in the governing equations and the use of the shell transformation to accurately model the open

boundary.

The observed discrepancy between the analytical benchmark and the Enhanced (`GetDP`) formulation (Figure 5.6)—amounting to approximately 12% in the $1000\,\Omega \cdot \mathrm{m}$ uniform soil case—is fundamentally attributable to the theoretical treatment of the longitudinal propagation constant (k_x). While the analytical formulation explicitly enforces a static assumption in the longitudinal direction ($k_x = 0$), the Enhanced formulation is derived from a generalized set of Maxwell's equations that implicitly captures longitudinal propagation effects. Consequently, even in the low-frequency regime, this rigorous inclusion leads to a divergence from the simplified analytical prediction, reflecting the Enhanced model's superior physical completeness.

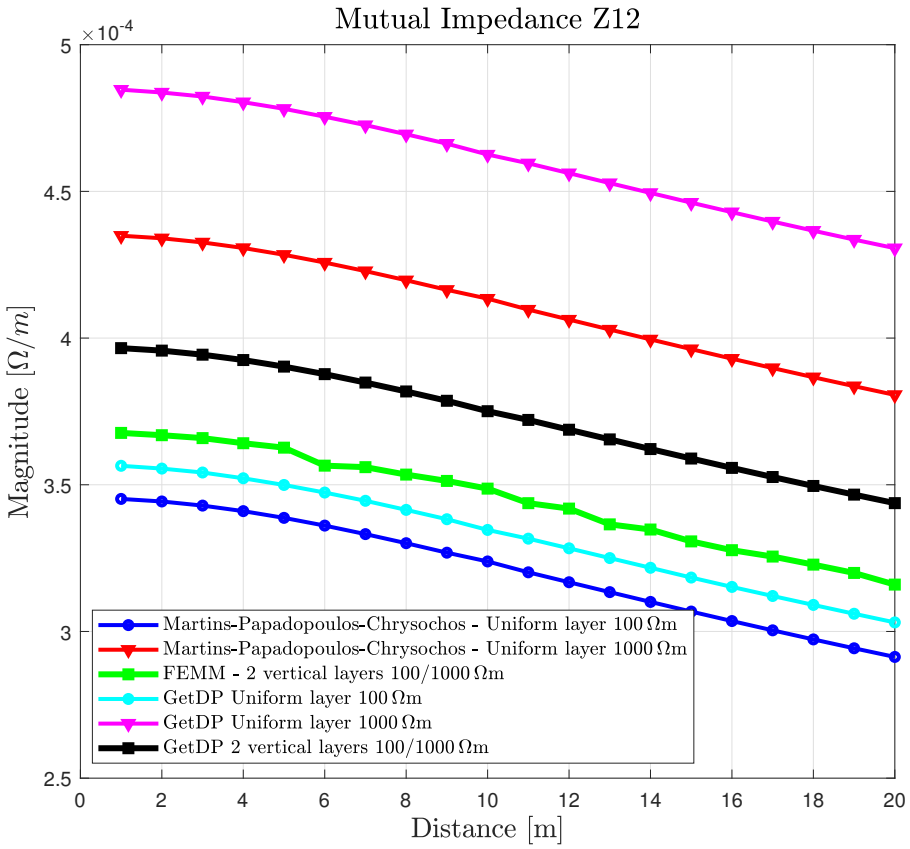

Figure 5.6. Mutual impedance between conductors 1 and 2 versus lateral distance d for vertically-layered and uniform soil models, considered at 60 Hz.

For the admittance, Figure 5.7, the difference is more clear. The results for vertical layer comparing `GetDP` and FEMM is of 22.5619 %, using (5.1). The results for the uniform soil cases, calculated using `GetDP`, demonstrate a direct proportionality between mutual impedance and soil resistivity. This is evidenced by the fact that the ration of impedance for the $\rho = 1000\ \Omega \cdot \mathrm{m}$ case and for the $\rho = 100\ \Omega \cdot \mathrm{m}$ case is approximately 10 which is the same ratio between

resistivity. The discrepancy in Y_{12} between the models stems from the inherent limitations of the analytical formulation (Section 3.1), specifically the numerical singularity present in the self-potential term P_{self} in Eq. 3.13.

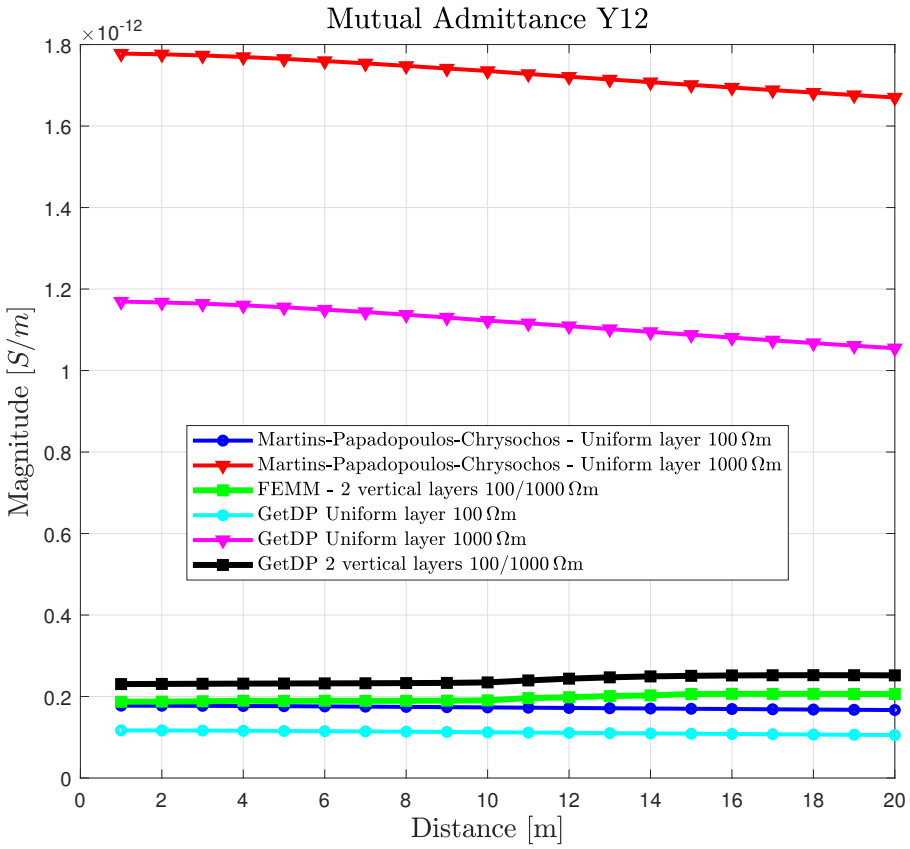

Figure 5.7. Mutual admittance between conductors 1 and 2 versus lateral distance d for vertically-layered and uniform soil models, considered at 60 Hz.

The mutual impedance $\mathbf{Z}_{12}$ from 0.1 Hz - 1 MHz is shown in Figure 5.8. Considering 5.1, calculating over the entire the frequency spectrum, the difference between the `GetDP` and FEMM for vertical layer is 0.4661 % and between uniform case is less than 5%. The results in lower frequency follows the pattern observed in Figure 5.6, `GetDP` formulation having a greater value than compared with analytical formulation and FEMM.

The mutual admittance $\mathbf{Y}_{12}$ from 0.1 Hz - 1 MHz is shown in Figure 5.9. Considering 5.1, calculating using the all the frequency spectrum, the difference between the `GetDP` and FEMM for vertical layer is 75.9 % which is very significant. For the case of $\rho = 100\ \Omega \cdot \mathrm{m}$ the difference between `GetDP` and FEMM is 15.4 %, and for $\rho = 1000\ \Omega \cdot \mathrm{m}$ 19.8 %. The results in lower frequency follows the pattern observed in Figure 5.7, analytical formulation having a greater value than compared with `GetDP`.

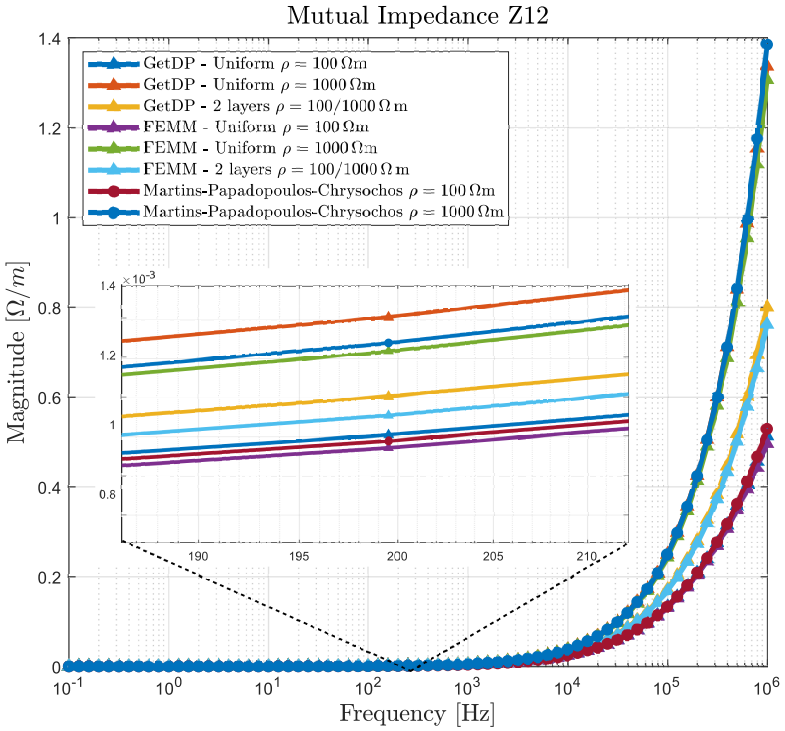

Figure 5.8. Mutual impedance between conductors 1 and 2 for different soil models.

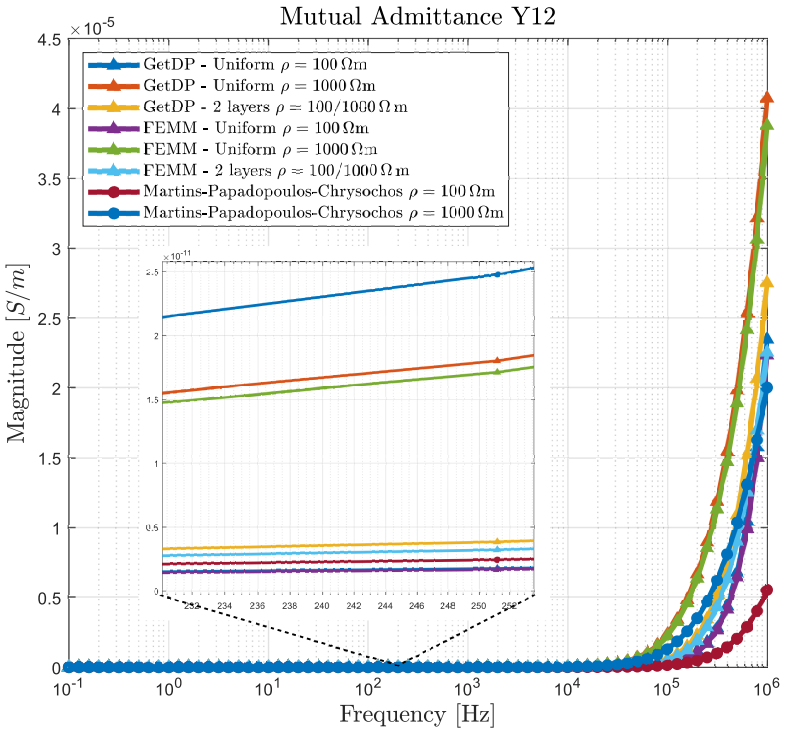

Figure 5.9. Mutual admittance between conductors 1 and 2 for different soil models.

5.2 CASE 2

To objectively assess the practical impact of lateral soil resistivity variations, an interference study is conducted on a system comprising a single-circuit overhead line with two shield wires and an underground pipeline within a two-layer soil structure, as shown in Figure 5.10. The parameters for the pipeline used in this simulation are provided in Table 5.2, based on data from (MARTINS-BRITTO CAIO M; RONDINEAU, 2020), and Table 5.3 the soil layers properties.

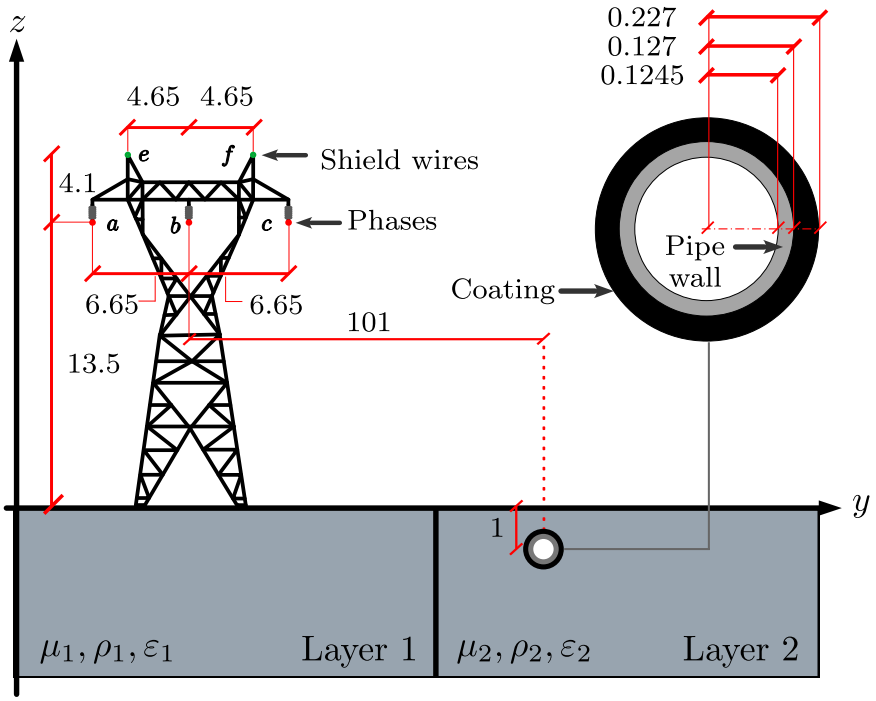

Figure 5.10. Cross-section of the system with overhead and underground conductors and two vertical soil layers.

5.2.1 Baseline formulation

Figure 5.11 shows the mesh generated by FEMM.

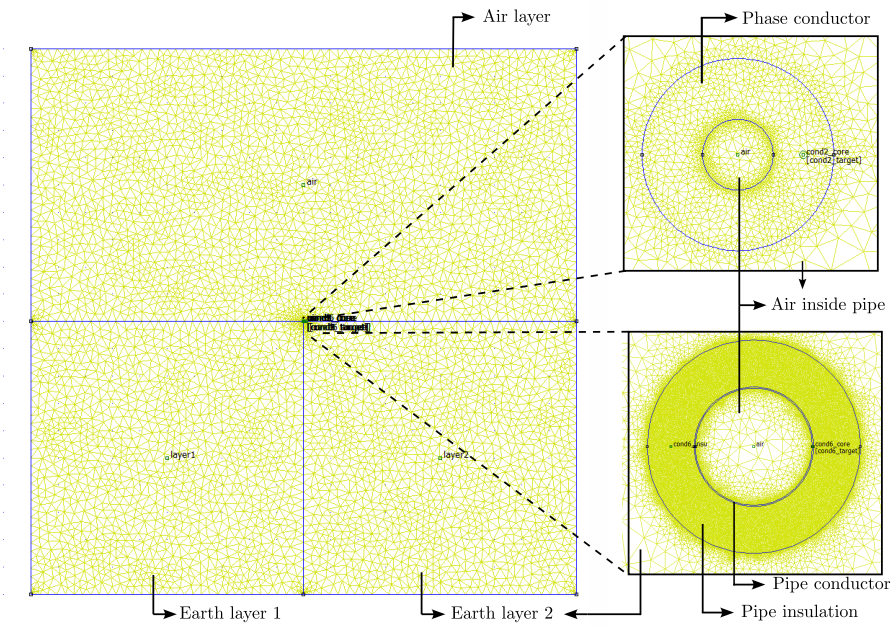

Figure 5.11. Cross-sectional view of the transmission line Mesh using FEMM.

Table 5.2. Pipeline characteristics.

Parameter	Value
Internal radius [m]	0.1245
External radius [m]	0.127
Insultation radius [m]	0.127
Electrical resistivity [Ω-m]	2.844×10^{-7}
Magnetic permeability [H/m]	3.142×10^{-4}
Coating resistivity $[\Omega\, m]$	10^{8}
Coating thickness [m]	0.1

Table 5.3. Electromagnetic properties of soil layers.

	Resistivity ρ [Ω·m]	**Permeability** μ [pu]	**Permittivity** ε [pu]
Uniform 1	100	1	15
Uniform 2	1000	1	15
Two layers	100/1000	1	15

The mutual impedances obtained for the system under investigation, described in Figure 5.12, show a similar trend as in the preceding section, i.e. the impedance of $Z^{FEM}_{\rho=1000} > Z^{FEM}_{\rho=100/1000} > Z^{FEM}_{\rho=100}$.

Additional simulations are conducted to calculate the pipeline induced voltages during the steady-state operation of the source circuit. Using the cross-section shown in Figure 5.10, an equivalent circuit representing a 2 km parallel exposure is modeled in ATP/ATPDraw,

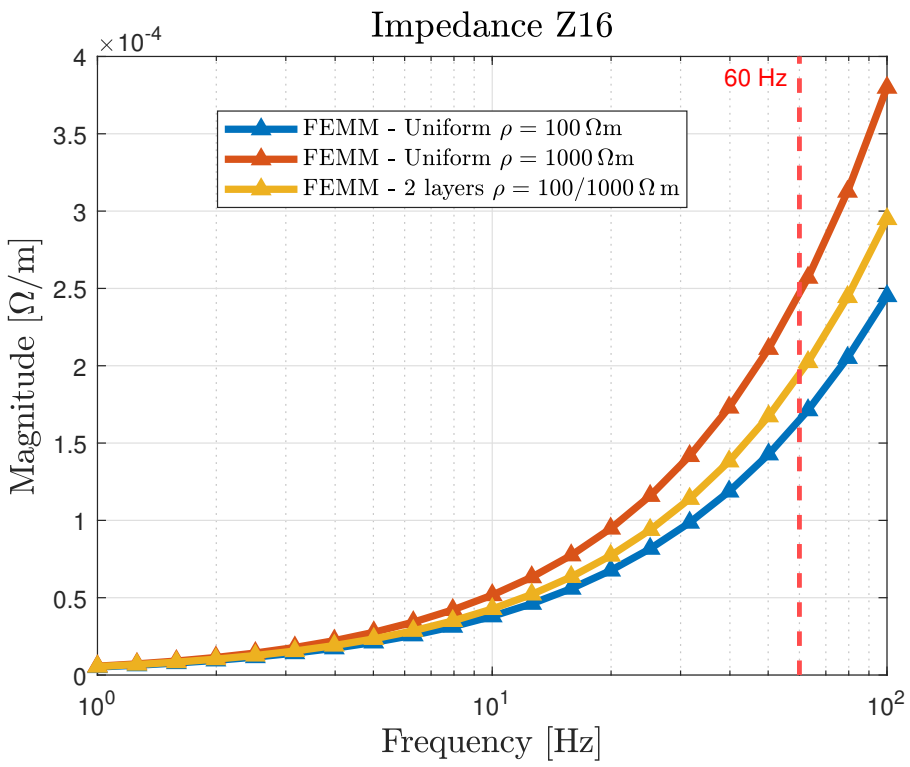

Figure 5.12. Mutual impedance between phase a (conductor 1) and the pipeline (conductor 6).

with the coupling effects represented by an external source representing the ground potential rise (GPR) and the tower grounding (Martins-Britto, 2020), according to Figure 5.13. Phase conductors, shield wires and the pipeline are almost matched by the corresponding characteristic impedances, through the resistances of 447, 517, and 56 Ω, respectively. The simulations are carried out with a sinusoidal voltage source at 60 Hz with 86.6 kV amplitude per phase in positive sequence using the LCC object set with the option "*Matrix Import*", which is a data format to recover externally calculated frequency-dependent arrays $\boldsymbol{Z}$ and $\boldsymbol{Y}$. Using the Universal line model (ULM), available in ATPDraw following the contribution of Zanon *et al.* (2021), the induced voltages are calculated at the beginning, middle, and end of the transmission line. The pipeline coating, GPR source, and tower grounding block shown in Figure 5.13 are created using the `LineCableLab` toolbox available in `amaurigmartins/LineCableLab`.

Figure 5.14 shows the magnitude of the RMS pipeline-induced voltage due to the magnetic coupling with the OHL. The resulting voltage profile follows the typical shape of an "V", as reported in previous literature reports for parallel exposures (MARTINS-BRITTO CAIO M; RONDINEAU, 2020; MARTINS-BRITTO LOPES; RONDINEAU, 2020; MICU *et al.*, 2013). In absolute terms, the voltage reaches its maximum at the pipeline endpoints and drops to zero

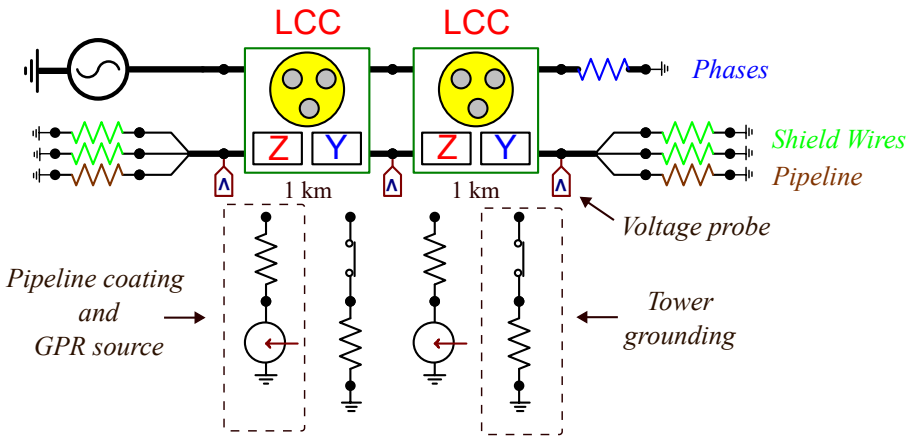

Figure 5.13. Equivalent circuit built in ATPDraw representing the coupling effects.

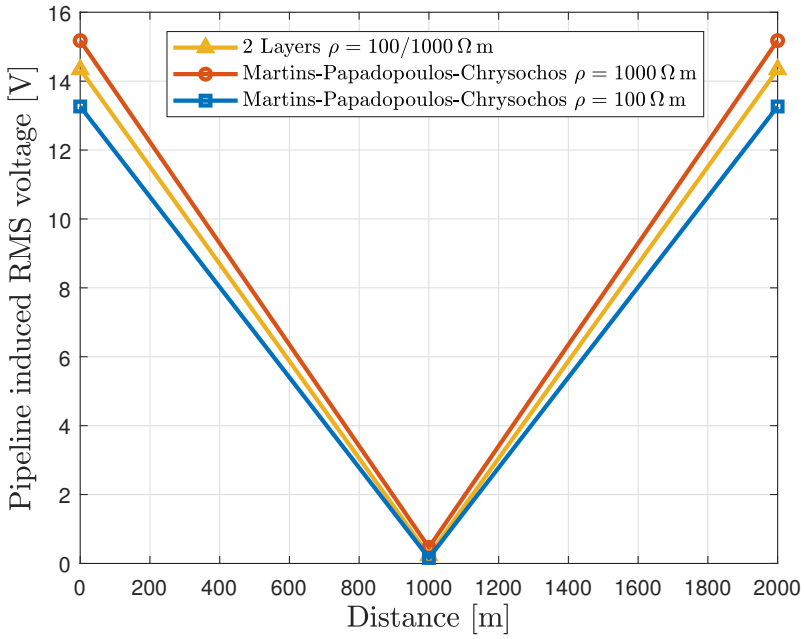

Figure 5.14. Pipeline induced voltage due to inductive coupling with OHL in a 2 km parallel exposure.

at its midpoint. Conversely, the induced current is expected to be maximum at the pipeline midpoint and minimum at the extremities. S

According to NACE SP0177-2014 (NACE International, 2014), the maximum allowable induced voltage on the pipeline is 15 V. For the two-layer vertical soil configuration, the induced voltage is 14.33 V. In contrast, the uniform soil model yields 15.17 V, as shown in Figure 5.14. Thus, the conservative uniform model approach exceeds the acceptable threshold, suggesting unnecessary mitigation measures that are not required for normal operation.

It is imperative to recognize that the operational integrity of a pipeline extends beyond the evaluation of steady-state induced voltages. A comprehensive interference analysis must pri-

oritize short-circuit conditions, where high-magnitude fault currents generate severe inductive coupling effects. Furthermore, the analysis must rigorously account for conductive coupling arising from the current through the transmission tower grounding systems. In scenarios of close proximity, the resulting Ground Potential Rise (GPR) can impose critical stress on the pipeline coating and creates direct arcing hazards. Consequently, effective mitigation strategies require a holistic assessment that integrates both transient fault scenarios and steady-state behavior. Nevertheless, the quantification of steady-state induced voltage remains a fundamental requirement for ensuring personnel safety during maintenance operations and for assessing the long-term risk of AC corrosion.

While the application study confirms that the baseline magnetostatic model is effective for low-frequency (60 Hz) impedance calculations and interference studies, its fundamental limitations remain. As demonstrated in the verification (Section 5.1.1), this FEMM formulation produced physically inconsistent results for the shunt admittance. Furthermore, its underlying magnetostatic assumption, which neglects displacement currents, inherently limits its applicability to low-frequency phenomena only.

To perform a comprehensive analysis across a wider frequency spectrum and to correctly model both the series impedance and the shunt admittance, a more robust formulation is necessary. The following section introduces an enhanced FEM model designed to overcome these specific limitations.

5.2.2 Enhanced formulation

For the application study, the system is modeled using the cross-section depicted in Figure 5.10. The corresponding finite element mesh, automatically generated by the toolbox `LineCableModels.jl`, is shown in Figure 5.15.

The calculated mutual impedance between phase a and the pipeline is presented in Figure 5.16. In this more complex scenario, the enhanced `GetDP` model predicts a higher impedance value compared to both the magnetostatic FEMM model and the analytical formulation due to the difference explain the previous sections.

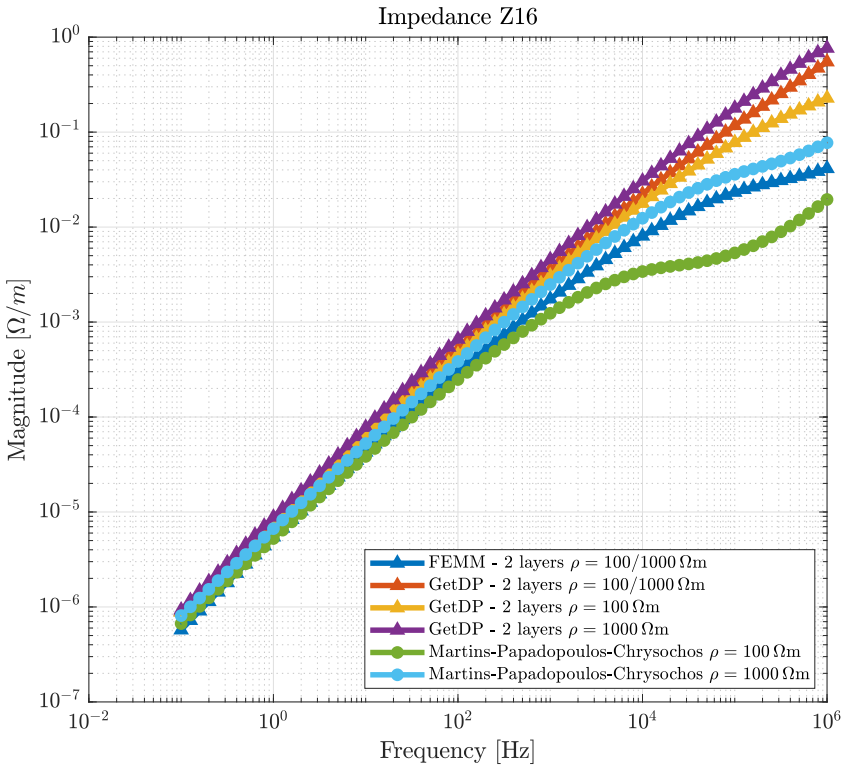

Figure 5.16. Mutual impedance between conductors 1 (phase a) and the pipe for different soil models.

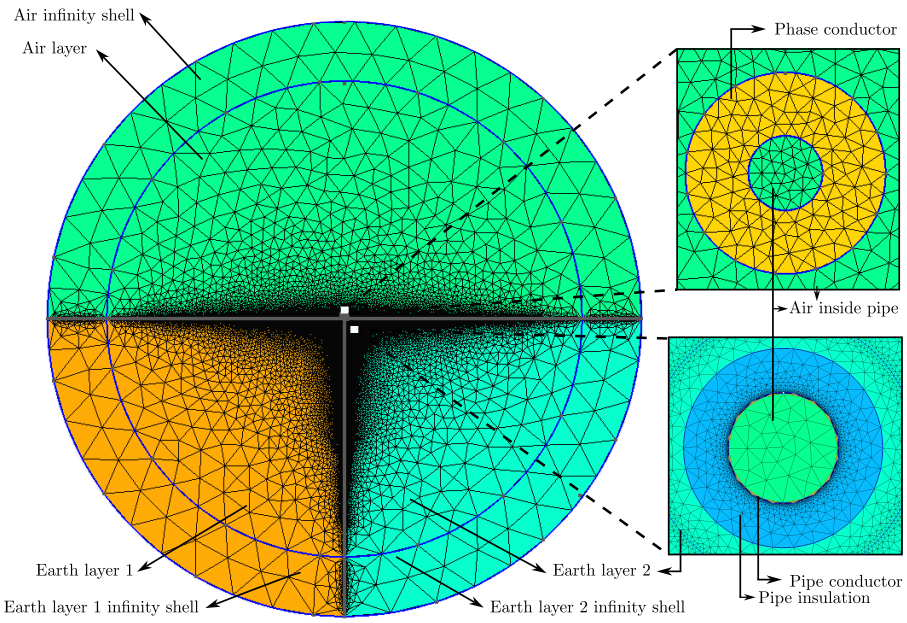

Figure 5.15. Cross-sectional view of the transmission line Mesh using *gmsh*.

As shown in Figure 5.17, the enhanced FEM model proposed in this chapter demonstrates a greater sensitivity to capacitive effects. The calculated admittance is not only higher in magnitude but also exhibits a clear frequency-dependent trend. The curve shows that the admittance value increases with frequency, a behavior that is consistent with theoretical ex-

pectations (where P defined in Eq. 3.11 are used to $Y = j\omega P$) and the results reported in the literature (MARTINS-BRITTO *et al.*, 2024).

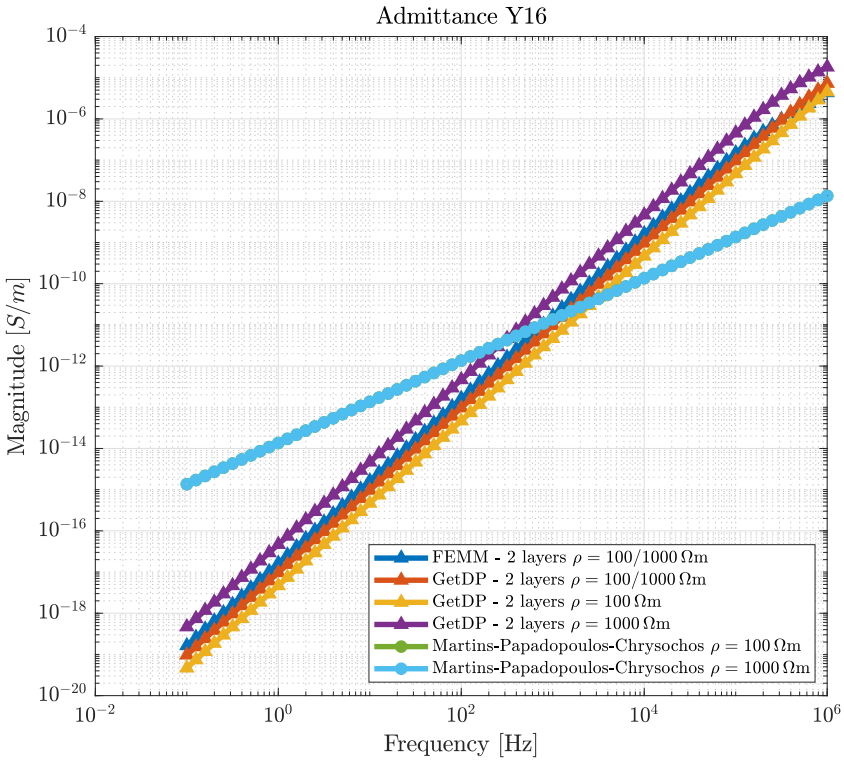

Figure 5.17. Mutual admittance between conductors 1 (phase a) and the pipe for different soil models.

5.3 CASE 3

The enhanced formulation presented in the last chapter proved to be a powerful tool for calculating earth return impedance and admittance. This case now applies this robust methodology to more complex configurations, such as underground and, most notably, submarine cables. The analysis of submarine cables is particularly critical given the rapid global expansion of offshore wind farms, which have gained prominence for both their clean energy and immense generating potential. According to the Global Wind Power Tracker, wind farms currently generate 1 TW of energy worldwide, with over 2.4 TW announced.

High-voltage submarine cables are the cornerstone of offshore wind projects, designed to transmit high power with minimal losses while withstanding the harsh maritime environment.

The computational domain used in this section is the same of the one in Section 4, following the skin depth of Earth in Eq.3.15

5.3.1 Verification case

To verify the enhanced formulation for multi-layer cables, the NA2XS(FL)2Y Cable from the manufacter is computed. This cable is build for 18 to 30 kV and is suitable for installation indoors, outdoors, in the ground and in water. Installation can be carried out in the ground or in a cable channel. The model used for this verification section is the of 1000 mm^2. Figure 5.18 shows the cable by a front view.

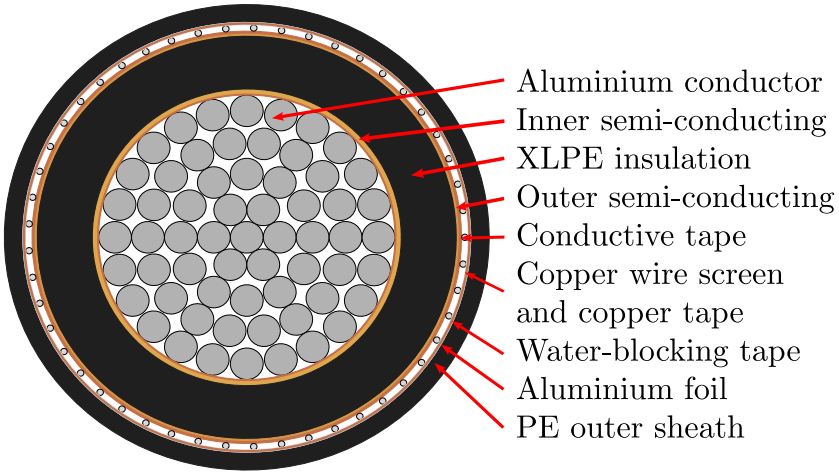

Figure 5.18. NA2XS(FL)2Y Cable.

The cable dimensions and materials was taken from Martins (2025), and are present in Table 5.4.

Table 5.5 presents the comparison between the manufacturer's specified p.u.l. parameters and the values computed by the FE model. The results for capacitance (C) show excellent agreement, with a relative error of only 5.5%, the computed series resistance (R) is 7.2% higher, and the series inductance (L) 1.0%. It is important to note that `GetDP` computes the series impedance and shunt admittance directly. Therefore, to facilitate comparison with the manufacturer's specifications, the equivalent resistance, inductance, and capacitance (RLC) parameters were derived from these complex quantities.

Overall, the small discrepancies between the simulated and specified values provide strong confidence in the model's accuracy. This results confirms that the enhanced formulation is a reliable tool for characterizing complex multilayer cables and can now be applied to more advanced studies.

Table 5.4. Geometric and material parameters of the MV 18/30kV 1000mm^2 cable (NA2XS(FL)2Y).

Layer / Component	Material	Parameter	Value [mm]
Core Conductor	Aluminum	Overall Diameter	38.1
		Wire Diameter	4.7
		Total Strands (Count)	61
Inner Semiconductive Tape	Polyacrylate	Thickness	0.3
Internal Semiconductor	Semicon	Thickness	0.6
Main Insulation	XLPE	Thickness	8.0
External Semiconductor	Semicon	Thickness	0.3
Outer Semiconductive Tape	Polyacrylate	Thickness	0.3
Wire Screen	Copper Wires	Wire Diameter	0.95
		Total Strands (Count)	49
Copper Tape	Copper	Thickness	0.1
Water Blocking Tape	Polyacrylate	Thickness	0.3
Laminated Tape	Aluminum/PE	Aluminum Thickness	0.15
		PE Face Thickness	0.05
Outer Jacket	Polyethylene (PE)	Thickness	2.4

Table 5.5. Parameter comparison.

Parameter	Datasheet	Computed	Error (%)
Resistance [Ω/km]	0.0291	0.027	7.2%
Inductance [mH/km]	0.3	0.297	1.0%
Capacitance [μF/km]	0.39	0.413	5.5%

The procedure for calculating the series impedance and shunt admittance of multi-layer cables requires an additional step. First, the impedance (Z) is calculated for each conductive component, and the admittance (Y) for each insulating component, resulting in a primitive matrix. Subsequently, applying Kron reduction and specific arithmetic operations as outlined by Ametani *et al.* (2022), these values are condensed into a single set of parameters for the cable. These equivalent parameters are then used for all subsequent analyses.

5.3.2 Enhanced formulation

This section evaluates the performance of a complex HVDC cable in a high-contrast environment. The system is modeled using a two-layer vertical configuration: the first layer represents typical soil ($\rho = 1000.0\,\Omega\cdot$m, $\varepsilon_r = 10$), and the second layer represents sea water ($\rho = 0.2\,\Omega\cdot$m, $\varepsilon_r = 81$). Although this specific configuration represents a theoretical benchmark rather than a

standard installation (which is not realistic), it is designed to rigorously investigate the impact of extreme resistivity contrast on the series impedance and shunt admittance, as well as its consequential effects on transient analysis.

To provide a comparison for the FEM results, the analytical formulation presented in Papadopoulos *et al.* (2010) was also computed using the `LineCableModels.jl` toolbox. The detailed cross-section of the HVDC cable used for this analysis is shown in Figure 5.19, and the cross-section is shown in Figure 5.20.

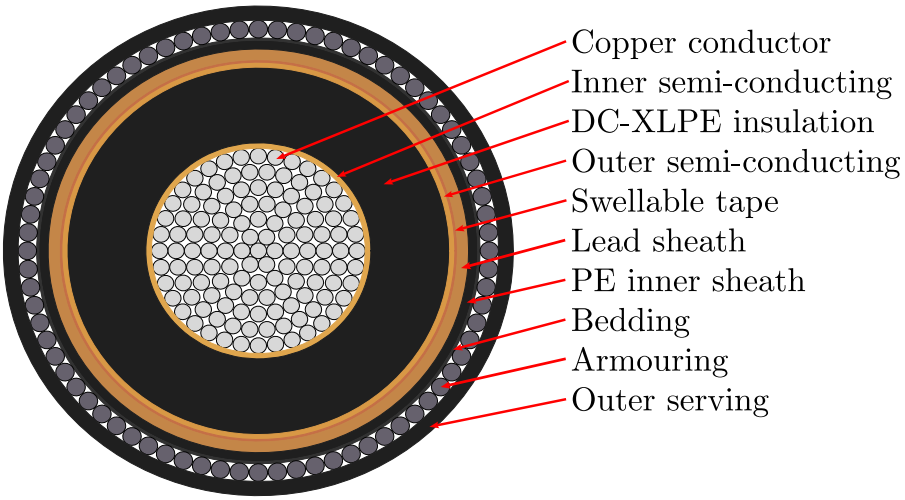

Figure 5.19. HVDC Cable up to 525 kV.

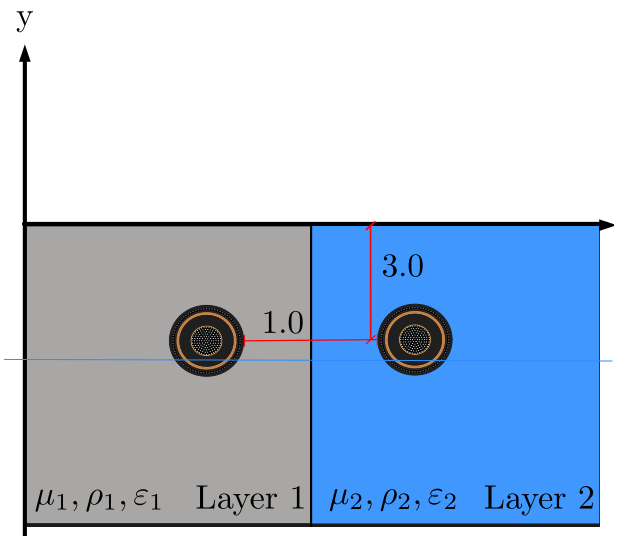

Figure 5.20. HVDC Cable cross-section.

The cable dimensions and materials was taken from Soares & Abrahamsson (2023), and are present in Table 5.6.

Table 5.6. Geometric and material parameters of the HVDC 525kV 2500mm^2 cable.

Layer / Component	Material	Parameter	Value
Core Conductor	Copper	Overall Diameter [mm]	57.8
		Number of Internal Layers	6
		Total Strands (Count)	127
Internal Semiconductor	Semicon	Thickness [mm]	1.5
Main Insulation	Polyethylene	Thickness [mm]	21.3
External Semiconductor	Semicon	Thickness [mm]	1.4
Water Blocking Tape	Polyacrylate	Thickness [mm]	0.7
Lead Sheath	Lead	Thickness [mm]	3.0
Inner Sheath	High-density Polyethylene	Thickness [mm]	2.5
Bedding	Polypropylene	Thickness [mm]	0.6
Armor	Steel Wires	Wire Diameter [mm]	5.0
		Total Strands (Count)	76
Outer Jacket	Polypropylene	Thickness [mm]	4.0

Figure 5.21 and 5.22 present the self and mutual impedance, respectively, while Figure 5.23 and 5.24 show the self and mutual admittance. All parameters are plotted on a log-log scale for better visualization, and are subscribed first number is with respect to the first cable and the second one for the second cable. Regarding the self-impedance, the analytical formulation's results are compared with the FEM simulations for the uniform soil cases ($\rho = 0.2\,\Omega \cdot \mathrm{m}$ and $\rho = 1000.0\,\Omega \cdot \mathrm{m}$). The analytical model consistently yields a higher value than the FEM.

For the mutual impedance, the value for the vertically layered model now stays lower than the uniform case for 1000.0 Ω-m. However, a new finding emerges at low frequencies (up to 100 Hz), where the impedance of the vertical layer model is actually higher than both uniform cases, exhibiting a distinct peak at approximately 10 Hz. The formulation preserves fundamental physical symmetries, as evidenced by the satisfaction of the reciprocity principle ($Z_{12} = Z_{21}$) across the entire frequency spectrum.

This low-frequency behavior is consistent with findings in (LORENZO *et al.*, 2023), which analyzed a 4-layer HVDC cable over horizontal layers of seawater and seabed. That study also reported a mutual impedance that was higher at low frequencies before decreasing as frequency increased, a phenomenon they attributed to the high conductivity (low resistivity) of the layers.

The self-admittance have a very similar results comparing with the Analytical formulation, but the mutual-admittance shows signs of numerical error in all models caused by low resistivity.

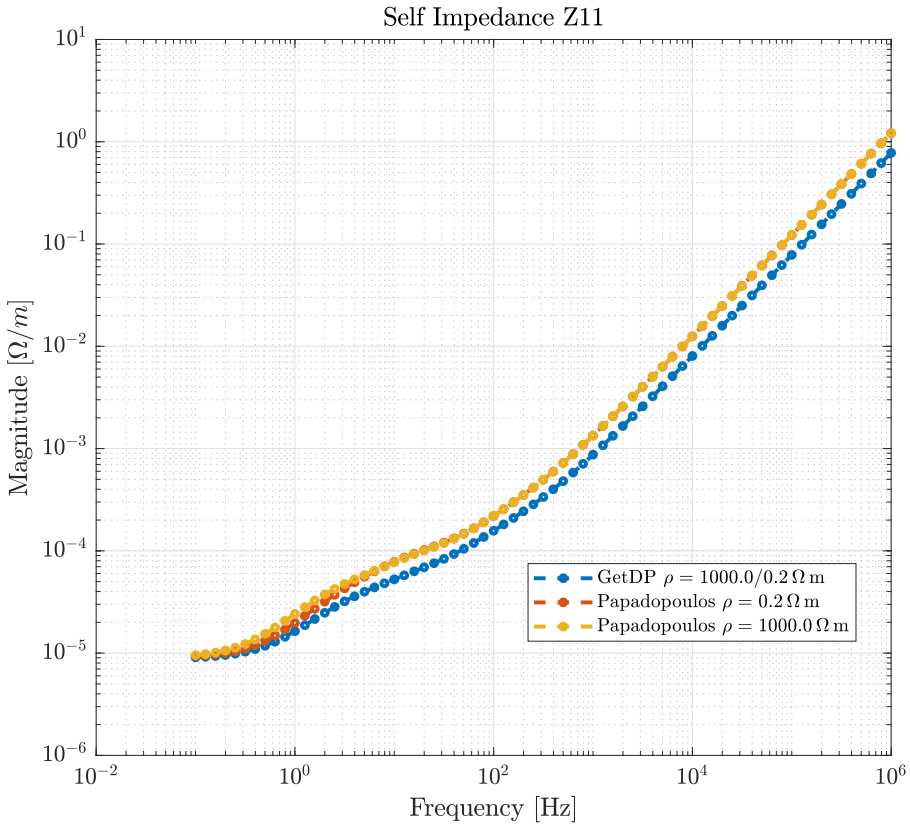

Figure 5.21. Self-impedance.

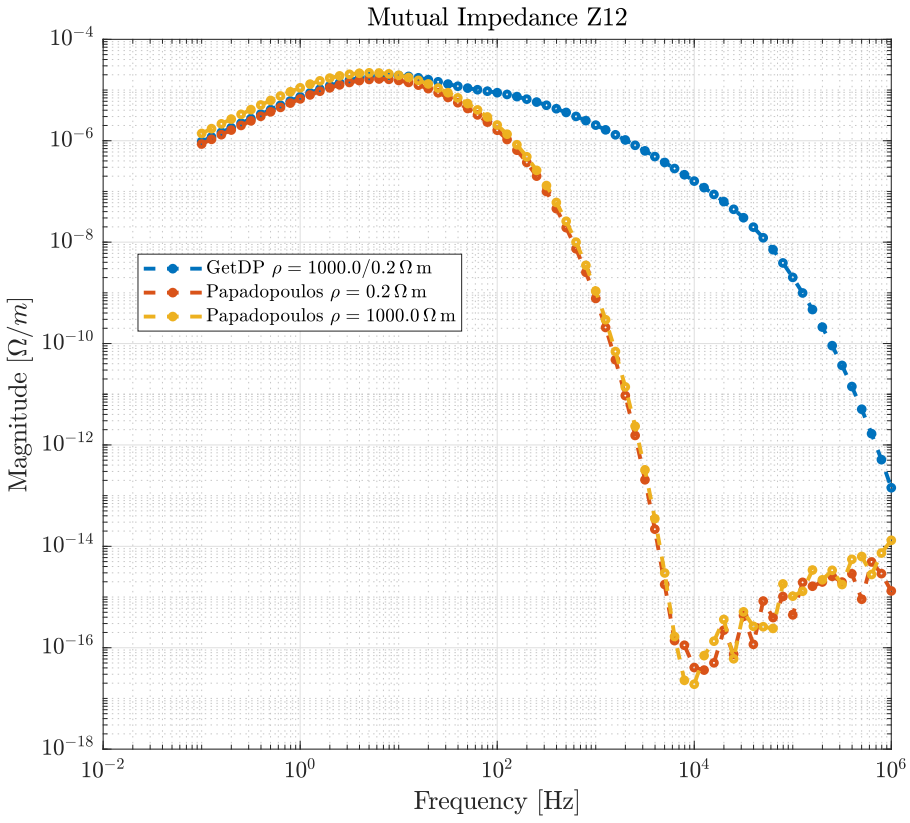

Figure 5.22. Mutual-impedance.

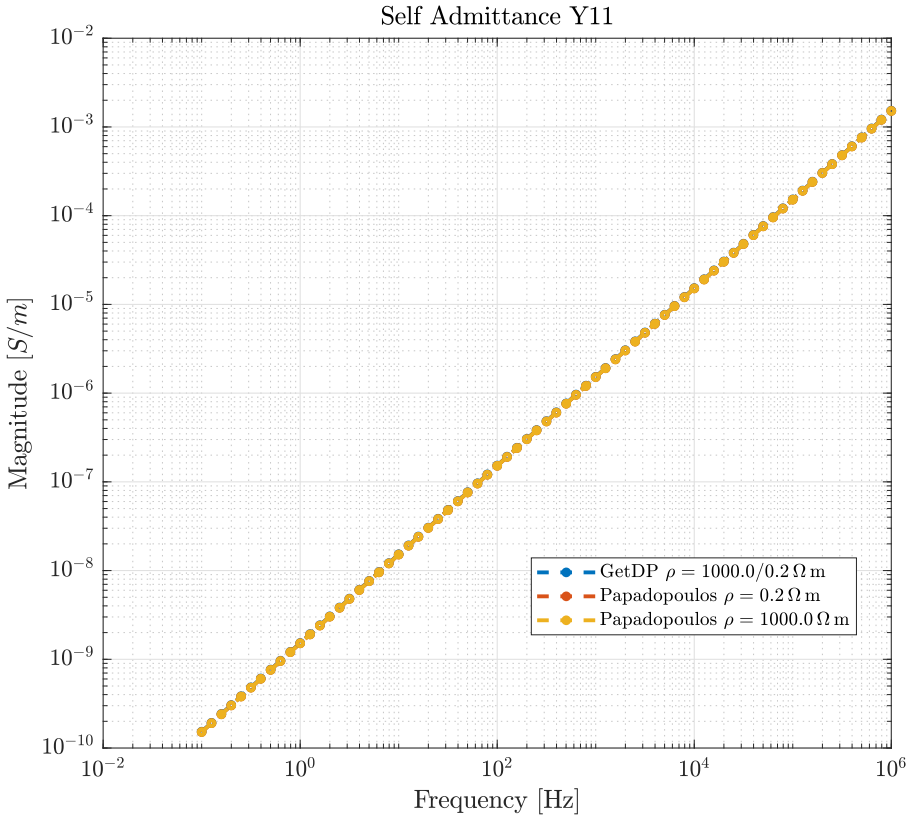

Figure 5.23. Self-admittance.

The mutual admittance shown in Figure 5.24 present a very low value, between 10^{-28} and 10^{-18}, and this is because of the layer with resistivity of 0.2 Ω-m it is a considerably conductive medium which acts like a electrostatic isolation for the other conductor.

The analysis was extended to the propagation parameters and characteristic impedance. The attenuation constant and phase velocity are plotted in Figure 5.25, and the characteristic impedance is shown in Figure 5.26. These parameters were calculated using the method from (CHRYSOCHOS *et al.*, 2014), which is based on the Levenberg-Marquardt optimization algorithm.

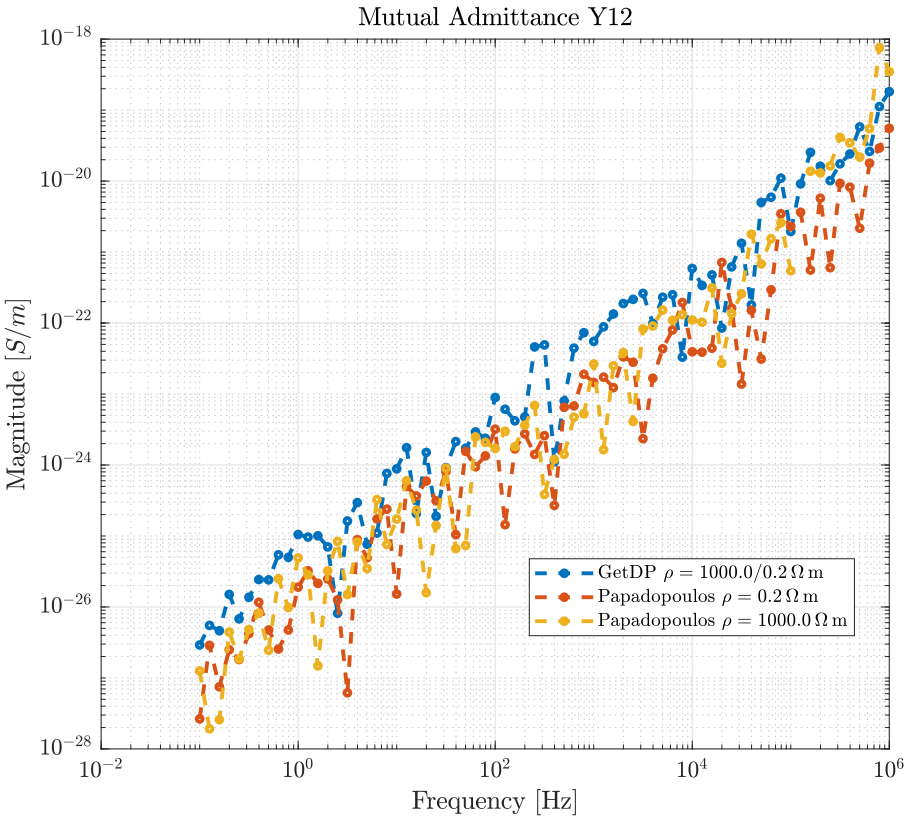

Figure 5.24. Mutual-admittance.

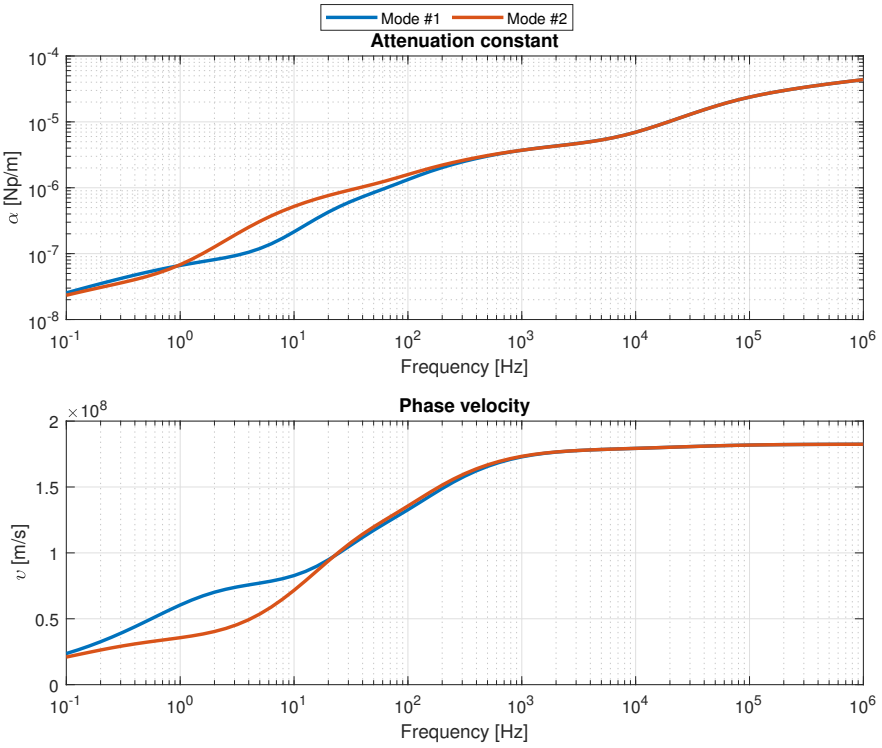

Figure 5.25. Attenuation constant and Phase velocity.

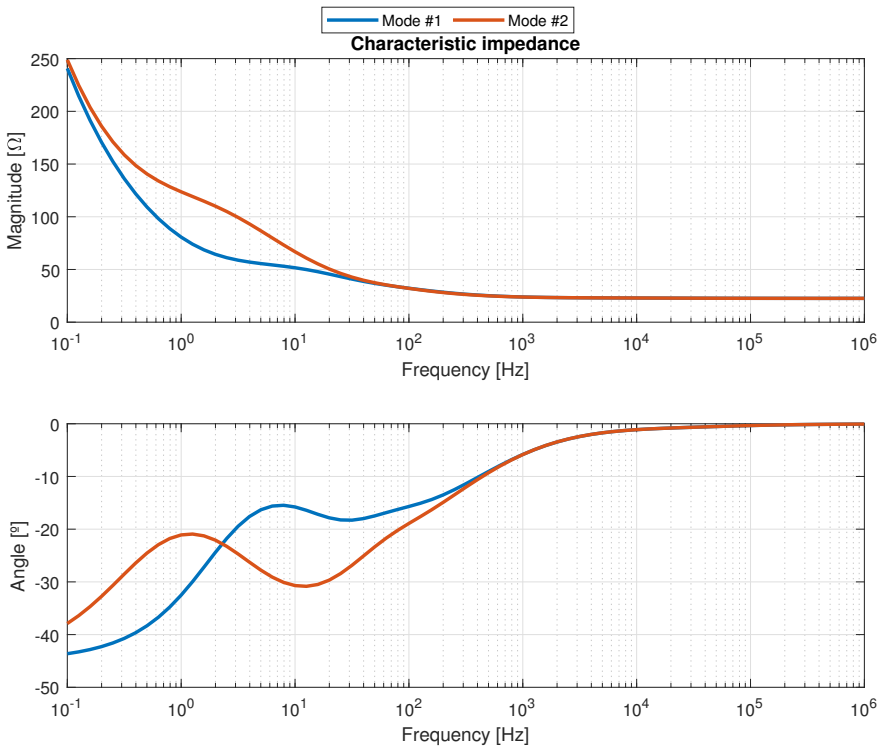

Figure 5.26. Characteristic impedance.

5.3.3 Transient Analysis

The transient analysis was simulated using PSCAD Software which uses the analytical aproximation of Deri-Semlyen for aerial, Saad for underground, and Lucca for mutual. The circuit is presented in Figure 5.27. The length used in the circuit was of 10 km, and a voltage source yielding a $1.2/50\ \mu_s$ double-exponential waveform of 1 per unit amplitude applied to the sending end of positive conductor pole.

In this simulation, the induced voltage at the receiving end of the negative conductor pole was evaluated for the Sheath, Armour, and Core. The analysis compares the vertically layered soil model against two uniform limiting cases with resistivities of $1000\,\Omega$-m and $0.2\,\Omega$-m. The results, presented in Figure 5.28, reveal a significant discrepancy between the induced voltages predicted by the vertical model and those from the two uniform models. This finding demonstrates that relying on simplified, uniform limiting cases does not necessarily translate into greater safety or reliability, highlighting that a realistic, heterogeneous soil model is the most appropriate approach for accurate analysis

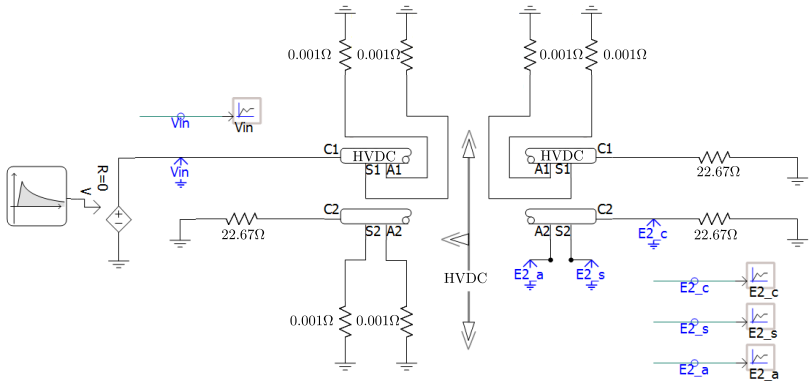

Figure 5.27. PSCAD schematic for transient analysis.

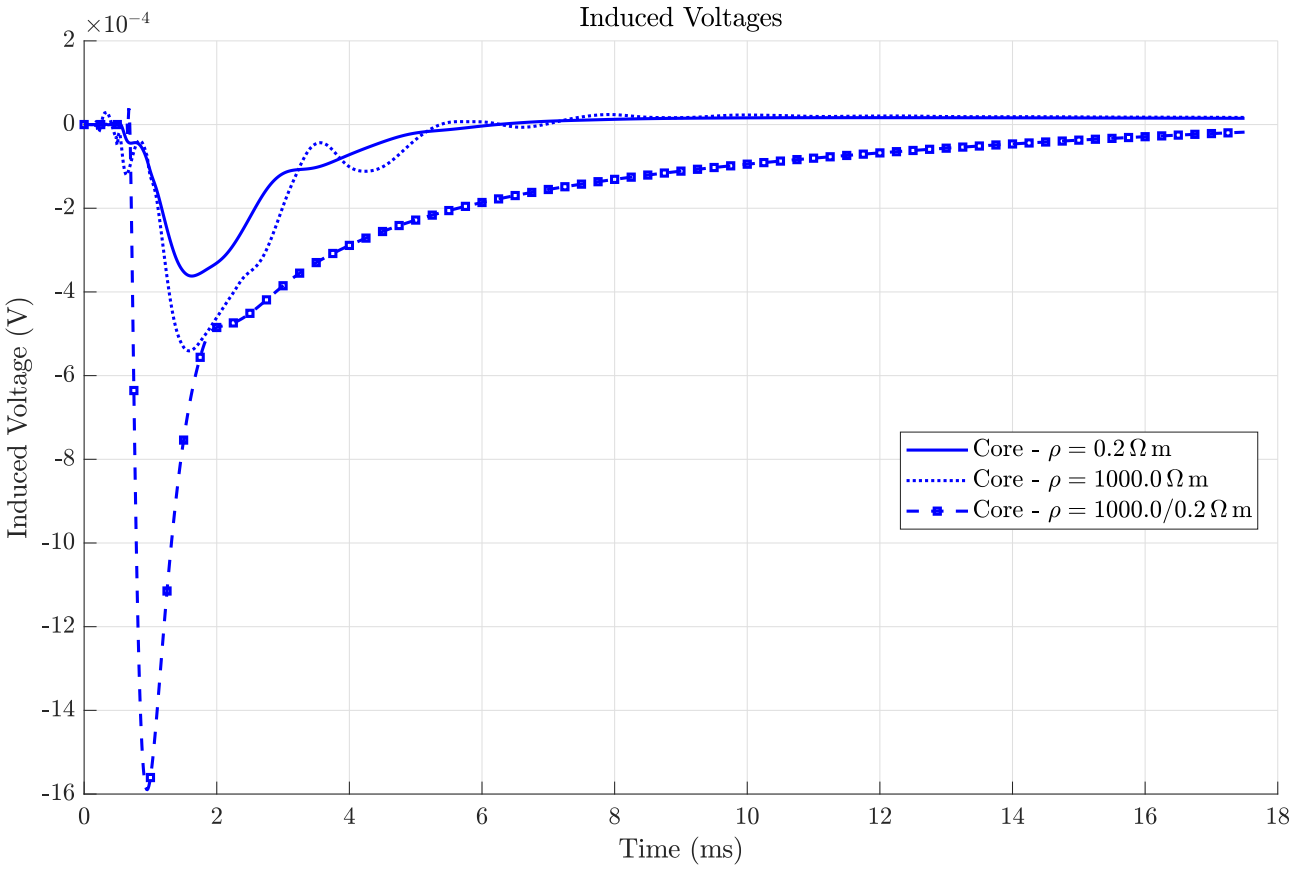

Figure 5.28. Transient analysis for $\rho = 0.2\,\Omega\,\mathrm{m}$, $\rho = 1000.0\,\Omega\,\mathrm{m}$ and $\rho = 1000.0/0.2\,\Omega\,\mathrm{m}$.

A simulation was performed in PSCAD to investigate the surge voltage behavior across the cable's conductive parts (Armour, Sheath, and Core). The analysis confirms two expected physical behaviors: first, the induced voltage is highest on the component closest to the surface (Armour > Sheath > Core), and second, the voltage magnitude is directly proportional to soil resistivity, with higher resistivity soil models yielding higher induced voltages (ZHANG *et al.*, 2011; LUCCA, 2019). When importing externally calculated line parameters into PSCAD, the

multi-component cable model (Core, Sheath, Armour) must be reduced to a single equivalent phase conductor. Since the import tool does not allow for the reconstruction of internal component voltages from this aggregated data, the analysis in Figure 5.29 plots the induced voltage for the Core only.

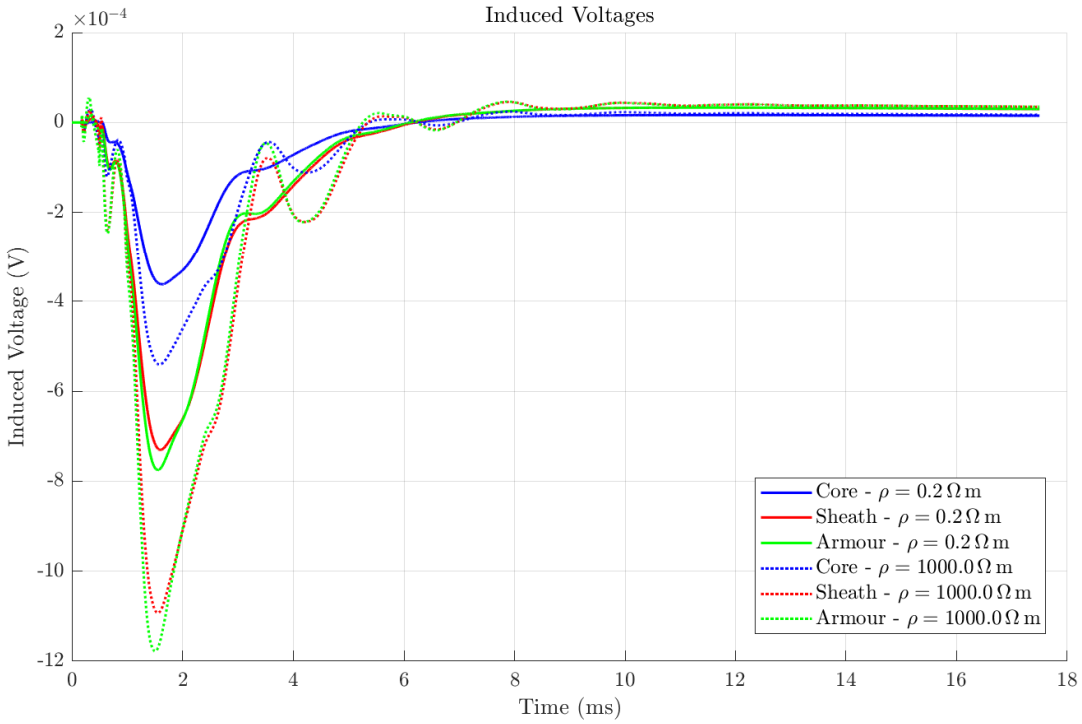

Figure 5.29. Transient analysis for $\rho = 0.2\,\Omega\,\mathrm{m}$ and $\rho = 1000.0\,\Omega\,\mathrm{m}$.

5.4 CHAPTER SUMMARY

This chapter presented a evaluation of the proposed FEM formulations through three progressive case studies, assessing the impact of lateral soil stratification on earth return parameters and electromagnetic interference.

First, a fundamental cross-sectional analysis served as a benchmark for verification. The investigation confirmed that while the Baseline magnetoquasistatic formulation provides reasonable impedance estimates at power frequency (60 Hz), it exhibits significant physical inconsistencies in shunt admittance calculations and fails to capture high-frequency phenomena. In contrast, the Enhanced formulation by accounting for displacement currents and dielectric effects demonstrated robust accuracy across a wide frequency spectrum (0.1 Hz to 1 MHz), producing admittance values consistent with theoretical expectations and analytical benchmarks.

Second, the methodology was applied to a practical AC interference scenario between an overhead transmission line and a buried pipeline. The results highlighted the economic and operational implications of soil modeling: the use of simplified uniform soil approximations resulted in an overestimation of induced voltages (RMSD of $\approx 19\%$), potentially triggering unnecessary and costly mitigation measures. The Enhanced formulation proved superior in capturing the frequency-dependent admittance profile essential for accurate coupling analysis.

Finally, the study culminated in the simulation of a complex HVDC submarine cable system. A critical contribution demonstrated in this section was the capability of the Enhanced formulation to explicitly model detailed multi-layer cable architectures—including individual conductor filaments—without the geometric simplifications typical of analytical approaches. Following a result against manufacturer datasheets (with deviations $< 7.2\%$), the formulation was applied to a high-contrast seabed environment. The subsequent transient analysis in PSCAD revealed that the surge response of systems in vertically stratified media differs fundamentally from uniform limiting cases, underscoring the necessity of heterogeneous soil modeling for the reliable insulation coordination of critical infrastructure. boundaries, preventing artificial constraints.

CHAPTER 6

CONCLUSION

This thesis addressed the computational challenges associated with the accurate determination of earth return parameters in complex, vertically stratified soil environments. The research was motivated by the limitations of traditional analytical formulations—which are fundamentally restricted to horizontally layered media—and the inadequacies of standard magnetoquasistatic (MQS) Finite Element approximations in high-frequency regimes. Through the development of two distinct computational formulations, this work established a rigorous methodology for analyzing electromagnetic interference and wave propagation in heterogeneous conductors and soils.

The primary scientific contributions and findings of this investigation are synthesized as follows:

1. **Impact of Lateral Soil Stratification:** The results consistently demonstrated that lateral soil heterogeneities (vertical stratification) exert a non-negligible influence on transmission line parameters. In both the fundamental case 1 and case 2, the response of the vertically stratified model did not merely oscillate between the values of the limiting uniform soil cases. Instead, it exhibited distinct physical behaviors that simplified uniform models failed to capture. Consequently, reliance on conservative uniform soil approximations can lead to significant errors in engineering judgment, such as the overestimation of induced voltages in pipelines (observed in Case 2), potentially necessitating unjustified and costly mitigation measures.

2. **Limitations of the Magnetoquasistatic Assumption:** The evaluation of the Baseline FEM formulation (implemented in FEMM) confirmed that while MQS assumptions are sufficient for series impedance calculations at power frequencies (50/60 Hz), they are structurally incapable of resolving shunt admittance or high-frequency phenomena. The

neglect of displacement currents in the diffusion equation led to physical inconsistencies in the calculated admittance, rendering the Baseline model unsuitable for transient analysis or wideband characterization.

3. **Computational Toolchain Development:** A distinct contribution of this work is the development of a high-performance, open-source scientific workflow. The creation of the `GetDP.jl` interface allows for the programmatic definition of Finite Element problems directly within the Julia environment. This architecture ensures reproducibility, facilitates parameter sweeps, and enables the seamless integration of electromagnetic field solving with circuit-theoretic analysis.

6.1 FUTURE WORK

- **Investigation of Numerical Instabilities in High-Contrast Media:** Detailed investigation into the numerical instabilities observed in the mutual admittance calculation for the HVDC case. These artifacts are hypothesized to stem from matrix ill-conditioning caused by the extreme conductivity contrast between the seawater layer (≈ 5 S/m) and the surrounding soil/insulation. Future work should focus on preconditioning techniques or adaptive mesh refinement to stabilize the solution in these low-resistivity regimes.

- **Expanded Transient Analysis:** Extension of the study scope to encompass a broader spectrum of transient events, including direct lightning strikes and complex switching operations. This will provide a more comprehensive quantification of how lateral soil stratification modifies surge propagation and attenuation compared to uniform soil assumptions.

- **Full-Wave Formulation:** Development of a Full-Wave Finite Element formulation to transcend the quasi-static limits entirely. This advancement would allow for the accurate modeling of electromagnetic phenomena across a significantly broader frequency spectrum, capturing radiation effects and wave propagation dynamics that become dominant at very high frequencies.

- **Multiphysics Coupling (Magneto-Thermal):** Development and integration of a ther-

mal solver within the Enhanced FEM formulation to create a coupled magneto-thermal simulation. This multiphysics approach would enable dynamic ampacity analysis, capturing the temperature dependence of material properties (e.g., the thermal coefficient of resistivity for conductors) and the heat dissipation characteristics of the stratified soil environment.

BIBLIOGRAPHY

AMETANI, A.; XUE, H.; OHNO, T.; KHALILNEZHAD, H. *Electromagnetic transients in large HV cable networks*. Stevenage, England: Institution of Engineering and Technology, 2022. (Energy Engineering). Citado 2 vezes nas páginas 1 and 44.

BATISTA, R.; PAULINO, J. O. S. Computing grounding resistance and impulse impedance of horizontal electrodes parallel or perpendicular to the interface of a vertically stratified soil using transmission line theory. *Electric Power Systems Research*, Elsevier, v. 194, p. 107060, 2021. Citado na página 9.

CARSON, J. R. Wave propagation in overhead wires with ground return. *The Bell System Technical Journal*, v. 5, n. 4, p. 539–554, 1926. Citado na página 1.

CHRYSOCHOS, A. I.; PAPADOPOULOS, T. A.; PAPAGIANNIS, G. K. Robust calculation of frequency-dependent transmission-line transformation matrices using the levenberg–marquardt method. *IEEE Transactions on Power Delivery*, v. 29, n. 4, p. 1621–1629, 2014. Citado na página 48.

DARWIN, C. G. Li. the dynamical motions of charged particles. *Philosophical Magazine Series 6*, Taylor Francis, v. 39, n. 233, p. 537–551, 1920. Citado 2 vezes nas páginas 12 and 21.

DERI, A.; TEVAN, G.; SEMLYEN, A.; CASTANHEIRA, A. The complex ground return plane a simplified model for homogeneous and multi-layer earth return. *IEEE Transactions on Power Apparatus and Systems*, PAS-100, n. 8, p. 3686–3693, 1981. Citado na página 2.

DOMMEL, H.; ADMINISTRATION, B. P. *Electromagnetic Transients Program Reference Manual: (EMTP) Theory Book*. Bonneville Power Administration, 1986. Disponível em: <https://books.google.com.br/books?id=CMHUnAEACAAJ>. Citado na página 1.

FREEMAN, E.; LOWTHER, D. An open boundary technique for axisymmetric and three dimensional magnetic and electric field problems. *IEEE Transactions on Magnetics*, v. 25, n. 5, p. 4135–4137, 1989. Citado 2 vezes nas páginas 23 and 24.

GEUZAINE, C. GetDP: a general finite-element solver for the de rham complex. *Proc. Appl. Math. Mech.*, Wiley, v. 7, n. 1, p. 1010603–1010604, dez. 2007. Citado 2 vezes nas páginas 19 and 24.

GEUZAINE, C.; REMACLE, J.-F.; DULAR, P. Gmsh: a three-dimensional finite element mesh generator. *International Journal for Numerical Methods in Engineering*, v. 79, n. 11, p. 1309–1331, 2009. Citado na página 19.

HAUBRICH, H.-J.; FLECHNER, B. A.; MACHCZYNSKI, W. A universal model for the computation of the electromagnetic interference on earth return circuits. *IEEE Trans. Power Deliv.*, Institute of Electrical and Electronics Engineers (IEEE), v. 9, n. 3, p. 1593–1599, jul. 1994. Citado na página 1.

HENROTTE, F.; MEYS, B.; HEDIA, H.; DULAR, P.; LEGROS, W. Finite element modelling with transformation techniques. *IEEE Transactions on Magnetics*, v. 35, n. 3, p. 1434–1437, 1999. Citado na página 23.

HUANG, Y.; TANG, B.; QU, Z.; CHEN, B. Fitting algorithm for power tower grounding resistance with vertical layered soil model. In: *2014 International Conference on Lightning Protection (ICLP)*. [S.l.: s.n.], 2014. p. 676–680. Citado na página 9.

IMHOFF, J.; MEUNIER, G.; BRUNOTTE, X.; SABONNADIERE, J. An original solution for unbounded electromagnetic 2d- and 3d-problems throughout the finite element method. *IEEE Transactions on Magnetics*, v. 26, n. 5, p. 1659–1661, 1990. Citado 2 vezes nas páginas iii and 23.

JIANG, L.; DONG, X.; ZHOU, X.; WANG, J.; SONG, J.; MA, Q. Propagation characteristics of lightning radiation field on three-layer vertical layered ground based on cpml absorption boundary. *IEEE Transactions on Electromagnetic Compatibility*, v. 65, n. 4, p. 1191–1201, 2023. Citado na página 9.

Kikuchi, H. Wave propagation along an infinite wire above ground at high frequencies. *Electrotech. J. Jpn.*, v. 2, p. 73–78, 1956. Citado na página 1.

LARSSON, J. Electromagnetics from a quasistatic perspective. *Am. J. Phys.*, American Association of Physics Teachers (AAPT), v. 75, n. 3, p. 230–239, mar. 2007. Citado na página 21.

LI, Z.-X.; FAN, J.-B.; CHEN, W.-J. Numerical simulation of substation grounding grids buried in both horizontal and vertical multilayer earth model. *International Journal for Numerical Methods in Engineering*, Wiley Online Library, v. 69, n. 11, p. 2359–2380, 2007. Citado na página 9.

LORENZO, G. D.; STRACQUALURSI, E.; MARZINOTTO, M.; FARIA, J. B.; ARANEO, R. Ground-return parameters of submarine cables buried in the seabed. *IEEE Transactions on Electromagnetic Compatibility*, v. 65, n. 2, p. 574–584, 2023. Citado na página 46.

LUCCA, G. Ac corrosion on pipelines: Influence of the surface layer soil resistivity in evaluating the current density by a probabilistic approach. *Prog. Electromagn. Res. M*, EMW Publishing, v. 79, p. 175–186, 2019. Citado na página 51.

MAGALHãES, A. P. C.; SILVA, J. C. L. V.; LIMA, A. C. S.; BARROS, M. T. Correia de. Validation limits of quasi-tem approximation for buried bare and insulated cables. *IEEE Transactions on Electromagnetic Compatibility*, v. 57, n. 6, p. 1690–1697, 2015. Citado na página 11.

MARTINS, A. *LineCableModels.jl: A Julia Package for Transmission Line and Cable Modeling*. 2025. <https://github.com/Electa-Git/LineCableModels.jl>. This work is supported by the Etch Competence Hub of EnergyVille, financed by the Flemish Government. The primary developer is Amauri Martins (@amaurigmartins), and the secondary developer is Lucas Lessa. Citado 3 vezes nas páginas 4, 19, and 43.

MARTINS, A.; LESSA, L. *GetDP.jl: A Julia Interface for the GetDP Finite Element Solver*. 2025. <https://github.com/Electa-Git/GetDP.jl>. This work is supported by the Etch Competence Hub of EnergyVille, financed by the Flemish Government. The primary developer

is Amauri Martins (@amaurigmartins) and the secondary developer is Lucas Lessa. This package is inspired by the pygetdp project. Citado na página 19.

Martins-Britto. *MODELAGEM DAS INTERFERÊNCIAS ELETROMAGNÉTICAS ENTRE LINHAS DE TRANSMISSÃO E TUBULAÇÕES METÁLICAS SUBTERRÂNEAS E ANÁLISE DE IMPACTOS*. Tese (Dissertaação de Mestrado) — Universidade de Brasília, Faculdade de Tecnologia, Departamento de Engenharia Elétrica, Distrito Federal, 2017. Citado na página 2.

Martins-Britto. *Realistic Modeling of Power Lines for Transient Electromagnetic Interference Studies*. xxiii, 157 p. Tese (Tese de Doutorado) — Universidade de Brasília, Faculdade de Tecnologia, Departamento de Engenharia Elétrica, Distrito Federal, 2020. 210 x 297 mm (ENE/FT/UnB, Doutor). Citado na página 38.

MARTINS-BRITTO; PAPADOPOULOS, T. A.; CHRYSOCHOS, A. I. Transient electromagnetic interference between overhead and underground conductors. *IEEE Transactions on Electromagnetic Compatibility*, v. 66, n. 3, p. 983–992, 2024. Citado 7 vezes nas páginas 1, 11, 12, 18, 30, 32, and 42.

MARTINS-BRITTO, A.; PAPADOPOULOS, T.; CHRYSOCHOS, A. *LineCableLab*. 2023. [Online]. Available: <https://www.mathworks.com/matlabcentral/fileexchange/130914-ohltoolbox>. Citado 6 vezes nas páginas 3, 9, 11, 13, 15, and 18.

MARTINS-BRITTO CAIO M, F. V. L.; RONDINEAU, S. Low-frequency electromagnetic coupling between a traction line and an underground pipeline in a multilayered soil. In: *2020 Workshop on Communication Networks and Power Systems (WCNPS)*. [S.l.: s.n.], 2020. p. 1–6. Citado 3 vezes nas páginas 2, 36, and 38.

MARTINS-BRITTO LOPES, F. V.; RONDINEAU, S. R. M. J. Multilayer earth structure approximation by a homogeneous conductivity soil for ground return impedance calculations. *IEEE Trans. Power Del.*, v. 35, n. 2, p. 881–891, 2020. Citado na página 38.

MEEKER, D. *Finite Element Method Magnetics Version 4.2 User's Manual*. 4th. ed. [S.l.], 2020. Available: <http://www.femm.info>. Citado 6 vezes nas páginas 3, 14, 15, 16, 17, and 18.

MICU, D. D.; CHRISTOFORIDIS, G. C.; CZUMBIL, L. Ac interference on pipelines due to double circuit power lines: A detailed study. *Electric Power Systems Research*, v. 103, p. 1–8, 2013. ISSN 0378-7796. Disponível em: <https://www.sciencedirect.com/science/article/pii/S0378779613001028>. Citado na página 38.

NACE International. *Mitigation of Alternating Current and Lightning Effects*. [S.l.]: NACE International, 2014. SP0177. Citado na página 39.

NAKAGAWA, M.; AMETANI, A.; IWAMOTO, K. Further studies on wave propagation in overhead lines with earth return: impedance of stratified earth. *Proceedings of the Institution of Electrical Engineers*, v. 120, p. 1521–1528, 1973. Disponível em: <https://digital-library.theiet.org/doi/abs/10.1049/piee.1973.0312>. Citado na página 2.

NAYEL, M. Numerical and experimnetal analysis of wenner method in two-horizontal and vertical layer ground. *JES. Journal of Engineering Sciences*, Assiut University, Faculty of Engineering, v. 42, n. 2, p. 385–396, 2014. Citado na página 9.

NAYEL, M. Study apparent grounding resistivity in vertical-layer soil. *Electric Power Components and Systems*, Taylor & Francis, v. 42, n. 8, p. 845–851, 2014. Citado na página 9.

NAYEL, M.; LU, B.; TIAN, Y.; ZHAO, Y. Study of soil resistivity measurements in vertical two-layer soil model. In: IEEE. *2012 Asia-Pacific Power and Energy Engineering Conference*. [S.l.], 2012. p. 1–5. Citado na página 9.

Papadopoulos, T. A.; Papagiannis, G. K.; Labridis, D. P. A generalized model for the calculation of the impedances and admittances of overhead power lines above stratified earth. *Electr. Power Syst. Res.*, v. 80, p. 1160–1170, 2010. Citado na página 1.

PAPADOPOULOS, T. A.; TSIAMITROS, D. A.; PAPAGIANNIS, G. K. Impedances and admittances of underground cables for the homogeneous earth case. *IEEE Transactions on Power Delivery*, v. 25, n. 2, p. 961–969, 2010. Citado 2 vezes nas páginas 11 and 45.

PAPADOPOULOS, T. A.; TSIAMITROS, D. A.; PAPAGIANNIS, G. K. Earth return admittances and impedances of underground cables in non-homogeneous earth. *IET Gener. Transm. Distrib.*, Institution of Engineering and Technology (IET), v. 5, n. 2, p. 161, 2011. Citado na página 11.

PAPAGIANNIS, G.; TRIANTAFYLLIDIS, D.; LABRIDIS, D. A one-step finite element formulation for the modeling of single and double-circuit transmission lines. *IEEE Transactions on Power Systems*, v. 15, n. 1, p. 33–38, 2000. Citado na página 3.

PAPAGIANNIS, G.; TSIAMITROS, D.; LABRIDIS, D.; DOKOPOULOS, P. A systematic approach to the evaluation of the influence of multilayered earth on overhead power transmission lines. *IEEE Transactions on Power Delivery*, v. 20, n. 4, p. 2594–2601, 2005. Citado 3 vezes nas páginas 3, 16, and 30.

POLLACZEK, F. Uber das feld einer unendlich langen wechselstromdurch-flossen einfachleitung. *ENT*, v. 3, n. 9, p. 339–360, 1926. Citado na página 1.

SOARES, T.; ABRAHAMSSON, A. *Submarine Cable Design Sheet - 1,250 MW*. [S.l.], 2023. Part of the Champlain Hudson Power Express project filing. Project ID: G22002. Citado na página 45.

TODD, D. K. *Groundwater Hydrology*. 2nd. ed. [S.l.]: Wiley, 2006. ISBN 9788126508365. Citado na página 6.

TRIANTAFYLLIDIS, D.; PAPAGIANNIS, G.; LABRIDIS, D. Calculation of overhead transmission line impedances a finite element approach. *IEEE Transactions on Power Delivery*, v. 14, n. 1, p. 287–293, 1999. Citado na página 16.

TSIAMITROS, D. A.; CHRISTOFORIDIS, G. C.; PAPAGIANNIS, G. K.; LABRIDIS, D. P.; DOKOPOULOS, P. S. Earth conduction effects in systems of overhead and underground conductors in multilayered soils. *IEE Proc. - Gener. Transm. Distrib.*, Institution of Engineering and Technology (IET), v. 153, n. 3, p. 291, 2006. Citado 2 vezes nas páginas 16 and 30.

WAIT, J. R. Theory of wave propagation along a thin wire parallel to an interface. *Radio Science*, v. 7, n. 6, p. 675–679, 1972. Citado na página 1.

WEDEPOHL, L.; WASLEY, R. Wave propagation in multiconductor overhead lines. calculation of series impedance for multilayer earth. *Proceedings of the Institution of Electrical Engineers*, v. 113, p. 627–632, 1966. Disponível em: <https://digital-library.theiet.org/doi/abs/10.1049/piee.1966.0102>. Citado na página 2.

WENNER, F. *A method of measuring earth resistivity*. [S.l.]: US Department of Commerce, Bureau of Standards, 1916. Citado na página 2.

WG-36.02, C. *Guide on the Influence of High Voltage AC Power Systems on Metallic Pipelines*. Paris, 1995. 26 p. Citado 2 vezes nas páginas 1 and 2.

Wise, W. H. Propagation of high-frequency currents in ground return circuits. *Proc. Inst. Radio Eng.*, v. 22, n. 4, p. 522–527, 1934. Citado na página 1.

XUE, H.; AMETANI, A.; MAHSEREDJIAN, J.; KOCAR, I. Generalized formulation of earth-return impedance/admittance and surge analysis on underground cables. *IEEE Transactions on Power Delivery*, v. 33, n. 6, p. 2654–2663, 2018. Citado na página 1.

XUE, H.; AMETANI, A.; MAHSEREDJIAN, J.; KOCAR, I. Generalized formulation of earth-return impedance/admittance and surge analysis on underground cables. *IEEE Transactions on Power Delivery*, v. 33, n. 6, p. 2654–2663, 2018. Citado na página 11.

ZANON, F. O.; LEAL, O. E.; De Conti, A. Implementation of the universal line model in the alternative transients program. *Electric Power Systems Research*, v. 197, p. 107311, 2021. ISSN 0378-7796. Disponível em: <https://www.sciencedirect.com/science/article/pii/S0378779621002923>. Citado na página 38.

ZENG, R.; HE, J.; GAO, Y.; ZOU, J.; GUAN, Z. Grounding resistance measurement analysis of grounding system in vertical-layered soil. *IEEE Transactions on Power Delivery*, v. 19, n. 4, p. 1553–1559, 2004. Citado na página 9.

ZHANG, H.; KARADY, G. G.; HUNT, J. Effect of various parameters on the inductive induced voltage and current on pipelines. In: *2011 IEEE Power and Energy Society General Meeting*. [S.l.: s.n.], 2011. p. 1–7. Citado na página 51.

ŞTEţ, D.; CZUMBIL, L.; MICU, D. D.; ŢOPA, V.; ANCAS, L. Stream gas pipeline in proximity of high voltage power lines. part i — soil resistivity evaluation. In: *2012 47th International Universities Power Engineering Conference (UPEC)*. [S.l.: s.n.], 2012. p. 1–5. Citado na página 9.